

Population modelling of FRBs from intrinsic properties

Mukul Bhattacharya,^{1*} Pawan Kumar,^{2†} and Duncan Lorimer^{3‡}

¹ *Department of Physics, University of Texas at Austin, Austin, TX 78712, USA*

² *Department of Astronomy, University of Texas at Austin, Austin, TX 78712, USA*

³ *Department of Physics and Astronomy, West Virginia University, Morgantown, WV 26506, USA*

Accepted . Received ; in original form

ABSTRACT

We develop a formalism to estimate the intrinsic properties of FRBs from observations by assuming a fixed DM contribution from a MW-like host galaxy, pulse temporal broadening models for turbulent plasma and a flat FRB energy spectrum. We then perform Monte Carlo simulations to constrain the properties of the FRB source, its host galaxy and scattering in the intervening plasma from the current observations. The typical scatter broadening of the intrinsic pulse is found to be considerably small $\lesssim 10^{-2}$ –1 ms with the ISM contribution suppressed significantly relative to IGM. The intrinsic width for non-repeating FRBs is broadened by a factor $\sim 2 - 3$ on average primarily due to dispersive smearing. The host galaxy DM contribution is likely to be smaller than the Galactic contribution and the FRB energy decreases significantly at high frequencies. We find that the FRB spatial density increases upto redshift $\sim 0.5 - 1.0$ and then drops significantly at larger distances. We obtain the energy distribution for FRB 121102 with repetition rate $\sim 0.1 - 0.3 \text{ hr}^{-1}$ and exponential energy cutoff that is significantly smaller compared to typical FRB energies. We find that the probability of observing none of the other FRBs to be repeating at Parkes is $\sim 0.8 - 1.0$ with the current follow-up data insufficient to suggest more than one class of FRB progenitors.

Key words: radio continuum: transients - cosmology: observations - scattering - turbulence - ISM: general

1 INTRODUCTION

Fast radio bursts (FRBs) are radio transients with millisecond duration and \sim Jy brightness, mostly detected from high Galactic latitudes (Lorimer et al. 2007; Thornton et al. 2013). The physical origin of these bursts is still unknown, primarily due to their short durations and the low angular resolutions of the current radio surveys. The frequency dependence of the arrival time delay ($\propto \nu^{-2}$) and the pulse width evolution ($\propto \nu^{-4}$) of FRBs are both consistent with propagation through cold, turbulent plasma suggesting their astrophysical origin. Until date, more than 50 non-repeating FRBs and two repeating FRBs have been published¹, and many more bursts are expected to be detected in the near future with the improving sensitivities of the upcoming radio transient surveys.

The cosmological origin of FRBs is strongly suggested by their large dispersion measures (integrated electron column density along the line of sight, $DM = \int n_e dl \sim 10^3 \text{ pc cm}^{-3}$), which typically exceeds the expected Galactic interstellar medium (ISM) contribution by almost an order of magnitude (Cordes & Lazio 2002). Assuming that most of the excess DM is due to the ionized intergalactic medium (IGM) contribution (Ioka 2003; Inoue 2004), the inferred redshifts are in the range $z \sim 0.2 - 2$ with a significant isotropic energy release of $\sim 10^{38} - 10^{40} \text{ erg}$ (Thornton et al. 2013; Keane & Petroff 2015; Champion et al. 2016). Due to their possible cosmological origin, FRBs can also be potentially used as a probe to study the distribution of free electrons in the IGM and cosmology (Gao et al. 2014; Zheng et al. 2014). The \sim ms pulse duration constrains the FRB source size, thereby implying high radio brightness temperatures and coherent emission (Katz 2014; Luan & Goldreich 2014).

Although the all-sky isotropic event rate for FRBs above fluence $\sim 1 \text{ Jy ms}$ is relatively high $\sim 10^3 - 10^4 \text{ day}^{-1}$ (Thornton et al. 2013; Champion et al. 2016; Rane et al. 2016), none of the FRBs except FRB 121102 (Scholz et

* E-mail: mukul.b@utexas.edu (MB)

† pk@astro.as.utexas.edu

‡ Duncan.Lorimer@mail.wvu.edu

¹ FRB catalogue lists the properties of all discovered FRBs (Petroff et al. 2016)

Table 1. Observed and inferred parameters for non-repeating FRBs published until January 2019 and with total DM exceeding 500 pc cm^{-3} . For each reported FRB, we select the observation with largest S/N from the [FRB catalogue](#). We place a lower DM cutoff for the FRBs considered in our analysis here to reduce the error in the estimates of the inferred parameters which are based on the assumption of the host galaxy DM contribution. We also exclude the FRBs with unresolved/imaginary intrinsic widths from our analysis (see equation 3). The definitions of all burst parameters are discussed in Section 2.

FRB	$S_{peak,obs}$ (Jy)	F_{obs} (Jy ms)	DM_{tot} (pc cm^{-3})	z	$L_{int1/2}$ (10^{44} erg/s)	E_{obs} (10^{42} erg)	w_{obs} (ms)	$w_{sc1/2}$ (ms)	$w_{int1/2}$ (ms)
010125	0.54	5.72	790.3	0.82	2.00/2.00	0.81	10.6	$1.10 \times 10^{-2}/1.94 \times 10^{-1}$	4.06/4.05
010621	0.53	4.24	748.0	0.20	0.11/0.11	0.03	8.0	$5.08 \times 10^{-4}/2.00 \times 10^{-2}$	2.93/2.93
090625	1.14	2.19	899.55	1.06	7.17/7.31	0.53	1.92	$3.64 \times 10^{-2}/2.98 \times 10^{-1}$	0.73/0.72
110220	1.11	7.31	944.38	1.12	6.35/6.35	1.94	6.59	$4.51 \times 10^{-2}/3.19 \times 10^{-1}$	3.06/3.05
110626	0.63	0.89	723.0	0.81	2.16/2.21	0.12	1.41	$1.13 \times 10^{-2}/2.04 \times 10^{-1}$	0.58/0.56
110703	0.45	1.75	1103.6	1.33	4.20/4.23	0.65	3.90	$9.45 \times 10^{-2}/4.01 \times 10^{-1}$	1.55/1.54
120127	0.62	0.75	553.3	0.61	0.97/0.98	0.06	1.21	$3.21 \times 10^{-3}/1.33 \times 10^{-1}$	0.60/0.59
121002	0.43	2.34	1629.18	2.00	11.19/11.23	1.86	5.44	$4.90 \times 10^{-1}/6.51 \times 10^{-1}$	1.66/1.66
130626	0.74	1.47	952.4	1.09	5.01/5.11	0.37	1.98	$3.99 \times 10^{-2}/3.07 \times 10^{-1}$	0.74/0.72
130729	0.22	3.43	861	1.01	0.97/0.97	0.75	15.61	$2.97 \times 10^{-2}/2.79 \times 10^{-1}$	7.73/7.73
131104	1.16	2.75	779	0.85	3.70/3.72	0.43	2.37	$1.41 \times 10^{-2}/2.19 \times 10^{-1}$	1.15/1.15
140514	0.47	1.32	562.7	0.62	0.63/0.63	0.11	2.82	$3.41 \times 10^{-3}/1.36 \times 10^{-1}$	1.68/1.68
150215	0.70	2.02	1105.6	0.82	2.08/2.09	0.28	2.88	$1.16 \times 10^{-2}/2.05 \times 10^{-1}$	1.37/1.37
151206	0.30	0.90	1909.80	2.28	20.63/20.13	0.90	3.0	$8.18 \times 10^{-1}/7.52 \times 10^{-1}$	0.44/0.45
151230	0.42	1.90	960.4	1.13	2.63/2.64	0.52	4.4	$4.81 \times 10^{-2}/3.25 \times 10^{-1}$	1.98/1.97
160317	3.0	63.00	1165	1.03	14.58/14.65	14.32	21.0	$2.58 \times 10^{-1}/1.90$	9.82/9.78
160608	4.3	38.70	682	0.51	3.79/3.80	2.05	9.0	$1.12 \times 10^{-2}/6.60 \times 10^{-1}$	5.40/5.38
170107	22.3	57.98	609.5	0.68	163.88/171.71	5.64	2.6	$5.76 \times 10^{-3}/1.73 \times 10^{-1}$	0.34/0.33
170416	19.4	97.00	523.2	0.56	22.06/22.07	6.30	5.0	$2.43 \times 10^{-3}/1.28 \times 10^{-1}$	2.86/2.86
170428	7.7	34.00	991.7	1.17	96.79/98.14	9.92	4.4	$6.16 \times 10^{-2}/3.74 \times 10^{-1}$	1.02/1.01
171116	19.6	63.00	618.5	0.69	60.58/60.93	6.32	3.2	$6.66 \times 10^{-3}/1.90 \times 10^{-1}$	1.04/1.04
180110	128.1	420.00	715.7	0.82	964.88/988.45	59.18	3.2	$1.38 \times 10^{-2}/2.42 \times 10^{-1}$	0.61/0.60
180131	22.2	100.00	657.7	0.74	56.54/56.64	11.46	4.5	$8.85 \times 10^{-3}/2.09 \times 10^{-1}$	2.03/2.02

al. 2016; Spitler et al. 2016) and FRB 180814.J0422+73 (CHIME/FRB Collaboration 2019) have been observed to repeat yet despite dedicated follow-up efforts (Petroff et al. 2015a; Ravi et al. 2015; Shannon et al. 2018). This might be due to two possible reasons: (1) two different classes of FRB progenitors (non-repeating and repeating bursts) as suggested by Keane et al. (2016), or (2) observational bias due to the finer localization and higher sensitivity of Arecibo and CHIME relative to Parkes. The repeating FRB 121102 has been localised to within $\sim 0.1''$ resolution with the Jansky VLA (Chatterjee et al. 2017) and is found to be associated to a dwarf star-forming host galaxy at $z=0.19273$ (Tendulkar et al. 2017) with a steady radio source at a separation of $\lesssim 0.01''$ determined with the European VLBI (Marcote et al. 2017).

Several progenitor models, including both cataclysmic and non-cataclysmic scenarios, have been proposed in the FRB literature: collapsing supermassive neutron stars (NSs;

Falcke & Rezzolla 2014; Zhang 2014), compact binary mergers (Piro 2012; Kashiyama et al. 2013; Totani 2013), galactic flaring stars (Loeb et al. 2014), radio emission from pulsar companions (Mottez & Zarka 2014), magnetar giant flares (Popov & Postnov 2010; Kulkarni et al. 2014; Lyubarsky 2014; Katz 2016), supergiant pulses from young pulsars (Connor et al. 2016; Cordes & Wasserman 2016; Lyutikov et al. 2016), young rapidly spinning magnetars (Kashiyama & Murase 2017; Metzger et al. 2017) and plasma stream interacting with NS magnetosphere (Zhang 2017). While most of the aforementioned models are primarily based on timescales and energetics considerations, Kumar et al. (2017) and Lu & Kumar (2018) have recently discussed the detailed calculations for the emission conditions and the plasma properties for coherent curvature radiation model. Here we concentrate only on the cosmological origin of FRBs as supported by the localisation of FRB 121102 at $z = 0.19273$. We consider the FRBs with total

DM ≥ 500 pc cm $^{-3}$ that were published until January 2019 for our analysis here. Unlike the previous population studies of FRBs, we derive the intrinsic properties of FRBs directly from observations.

In this study, we first develop a formalism to estimate the intrinsic properties of the non-repeating and repeating burst populations from the current observations. We then perform Monte Carlo (MC) simulations based on these intrinsic properties to constrain the scattering properties of the intervening IGM and ISM, FRB spatial density as a function of z , host galaxy DM and the spectral index of the assumed power-law FRB energy density. We also discuss whether the repeating FRB 121102 is representative of the entire FRB population based on its repeating behaviour and the follow-up observations for the non-repeating FRBs. This paper is organised as follows. In Section 2, we estimate the distances and intrinsic widths for the FRBs using appropriate models for the IGM and ISM properties, and further evaluate the energies and luminosities for these bursts. We then describe our MC code in Section 3 and discuss the simulation results in Section 4. We constrain the model parameters for the FRB population using the current observations. In Section 5, we investigate whether the repeating FRB 121102 is representative of all FRBs, and finally present our summary and conclusions in Section 6.

2 FRB INTRINSIC PARAMETERS FROM OBSERVABLES

In this section, we first estimate the distances to the observed FRBs from their total dispersion measure (DM_{tot}) by assuming a fixed host galaxy DM contribution (DM_{host}). We then obtain the intrinsic pulse widths (w_{int}) from the observed FRB widths (w_{obs}) using scattering models for the pulse temporal broadening due to the multipath propagation through the ionized ISM and IGM. The burst luminosities and energies are calculated for a flat energy spectrum from the peak flux density, distance and the frequency range for FRB radio emission. We study the correlation between the intrinsic parameters and the relative contributions from different width components.

2.1 Distance and width estimates

The total DM for any FRB has contributions from the IGM (DM_{IGM}), the Milky Way (MW) ISM (DM_{MW}) and the host galaxy ISM. Including the cosmological expansion factor for the host galaxy contribution gives

$$DM_{tot} = DM_{IGM} + DM_{MW} + \frac{DM_{host}}{(1+z)} \quad (1)$$

The IGM contribution increases with the source redshift as (Ioka 2003; Inoue 2004; Deng & Zhang 2014)

$$DM_{IGM} = \frac{c}{H_0} \int_0^z \frac{f_{IGM} n_e(z') x(z') dz'}{(1+z')^2 [\Omega_m(1+z')^3 + \Omega_\Lambda]^{0.5}} \\ = (1294.9 \text{ pc cm}^{-3}) \int_0^z \frac{(1+z') dz'}{\sqrt{(1+z')^3 + 2.7}} \quad (2)$$

where $f_{IGM} = 0.83$ is the fraction of baryon mass in the IGM, $n_e(z) = 2.1 \times 10^{-7} (1+z)^3 \text{ cm}^{-3}$ is the number density of free electrons, $x(z) \approx 7/8$ is the ionization fraction with

cosmological parameters as $H_0 = 68 \text{ km s}^{-1} \text{ Mpc}^{-1}$, $\Omega_m = 0.27$ and $\Omega_\Lambda = 0.73$.

The DM contribution from the Galactic ISM along the FRB source line of sight is obtained from the NE2001 model (Cordes & Lazio 2002). The host galaxy DM contribution depends on the type of the galaxy, location of the FRB source within the galaxy as well as our viewing angle relative to the galaxy. Although the host galaxy for the repeating FRB 121102 has been identified to be a dwarf star-forming galaxy (Tendulkar et al. 2017), there is still no information about the host galaxies for the other sources. Due to the uncertainties associated with the host galaxy properties and the FRB source location inside them, here we assume that the host galaxy has a free electron density distribution similar to that of the MW with a typical contribution of $DM_{host} \approx 100 \text{ pc cm}^{-3}$. With the values of DM_{tot} , DM_{MW} and DM_{host} known, we solve for the redshifts of the non-repeating bursts from equation (1). As the host galaxy for the repeating FRB 121102 is localized at $z=0.19273$ (Tendulkar et al. 2017), the DM_{IGM} value is precisely known and equation (1) further gives $DM_{host} \approx 281 \text{ pc cm}^{-3}$. Once z is estimated, the comoving distance to the source is obtained as $D(z) = (8.49 \text{ Gpc}) \int_0^z [(1+z')^3 + 2.7]^{-0.5} dz'$ with a luminosity distance $D_L(z) = (1+z)D(z)$.

The intrinsic width of a cosmological FRB source is broadened due to both propagation and telescope effects. Excluding the pulse broadening components from the observed width gives

$$w_{int}^2 = \frac{w_{obs}^2 - (w_{DM}^2 + w_{samp}^2 + w_{IGM}^2 + w_{ISM,MW}^2)}{(1+z)^2} - w_{ISM,host}^2 \quad (3)$$

where, $w_{DM} = 8.3 \times 10^6 (DM_{tot} \Delta\nu / \nu_0^3) \text{ ms}$, is the dispersive smearing across single frequency channels with $\Delta\nu$ and ν_0 being the channel bandwidth and the central frequency of observation in MHz, respectively. While w_{samp} is the sampling time of the observation, $w_{IGM}/w_{ISM,MW}/w_{ISM,host}$ denotes the pulse temporal broadening due to scattering in the IGM/MW ISM/host galaxy ISM and $(1+z)$ is the cosmic expansion factor.

As the radio pulses propagate through the ionised plasma in the intervening IGM and ISM, they are scattered due to the inhomogeneities in the electron density along the line of sight resulting in multipath propagation and thereby scatter broadening. The reported scattering timescales are significantly larger compared to the scattering timescales expected from the Galactic turbulence along such lines of sight and it is expected that most of the scattering is predominantly due to the IGM (Williamson 1972; Macquart & Koay 2013). Due to the absence of sufficient information on the FRB scattering timescales, we consider two models to evaluate the ISM and IGM scattering broadening timescales for each FRB as discussed below.

(i) *Scattering model 1:* We assume that the temporal broadening $w_{ISM,host/MW}$ due to scattering in the host galaxy/MW ISM is related to $DM_{host/MW}$ as given by the empirical fit obtained by Krishnakumar et al. (2015),

$$w_{ISM,host/MW} = (4.1 \times 10^{-8} \text{ ms}) 4f(1-f) \\ \times (1.00 + 1.94 \times 10^{-3} DM_{host/MW}^{2.0}) \frac{DM_{host/MW}^{2.2}}{\nu_{0,GHz}^{4.4}} \quad (4)$$

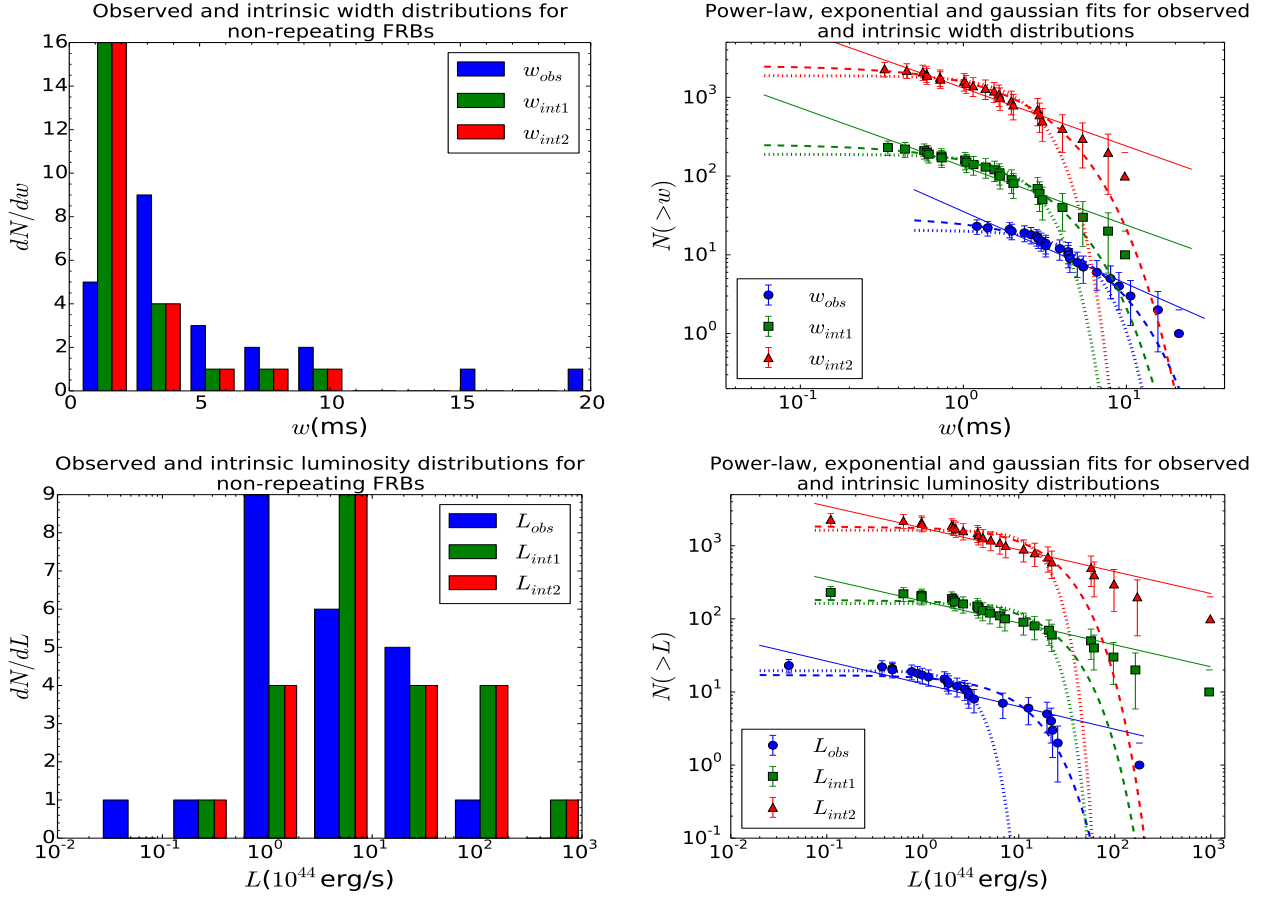


Figure 1. Pulse width and luminosity distributions for non-repeating bursts: Top-left panel: Histograms for widths w_{obs} , w_{int1} and w_{int2} , Top-right panel: Chi-squared fits for cumulative distributions of w_{obs} , w_{int1} and w_{int2} , Bottom-left panel: Histograms of luminosities L_{obs} , L_{int1} and L_{int2} , Bottom-right panel: Chi-squared fits for cumulative distributions of L_{obs} , L_{int1} and L_{int2} . The index 1/2 for the burst parameters denotes scattering model 1/2. The functional forms used for the chi-squared fits of the cumulative distributions are power-law, exponential and gaussian (see Table A2).

where $\nu_{0,GHz} = \nu_0/10^3$ is the central frequency in GHz and $4f(1-f)$ is the lever-arm factor by which $w_{ISM,host/MW}$ is suppressed. We use $f = 25 \text{ kpc}/D_L$, where D_L is the luminosity distance (in kpc) from the source to the observer and 25 kpc is the typical extent of a MW-like galaxy. Although most of the scattering material is present in the ISM of the host galaxy or the MW, their contribution to scatter broadening is expected to be significantly suppressed by a factor $4f(1-f) \sim 10^{-4}$ due to the asymmetric placement of the scattering screens relative to the source and the observer (Williamson 1972; Vandenberg 1976; Lorimer et al. 2013). As the average electron density fluctuations in the IGM are expected to be less significant compared to the ISM, we assume that the scatter broadening due to IGM can be obtained by rescaling the ISM contribution by three orders of magnitude (Lorimer et al. 2013; Caleb et al. 2016),

$$w_{IGM} = (4.1 \times 10^{-11} \text{ ms}) (1.00 + 1.94 \times 10^{-3} DM_{IGM}^{2.0}) \times \frac{DM_{IGM}^{2.2}}{\nu_{0,GHz}^{4.4}} \quad (5)$$

As opposed to the host galaxy/MW ISM scattering, IGM scattering is unaffected by geometrical effects such as the

lever-arm effect.

(ii) *Scattering model 2:* In this model, we assume that the ISM scatter broadening contribution from the host galaxy and the MW are still given by the $w_{ISM} - DM$ relation in equation (4). However, instead of rescaling $w_{ISM,host/MW}$ to obtain w_{IGM} , we use the theoretical temporal smearing expression for IGM turbulence as obtained by Macquart & Koay (2013),

$$w_{IGM}(z) = \frac{k_{IGM}}{\nu_{0,GHz}^4 Z_L} \int_0^z \frac{dz'}{[\Omega_m(1+z')^3 + \Omega_\Lambda]^{0.5}} \times \int_0^z \frac{(1+z')^3}{[\Omega_m(1+z')^3 + \Omega_\Lambda]^{0.5}} dz' \quad (6)$$

where $Z_L = (1+z)^2 \left[(1+z) - \sqrt{z(1+z)} \right]^{-1}$ and k_{IGM} is the normalisation factor (see Appendix A for a detailed derivation of equation 6). We fix the value of $k_{IGM} = 2.94 \times 10^{12} \text{ ms MHz}^4$ from equation (3) such that $w_{int} \leq \sqrt{w_{obs}^2 - (w_{DM}^2 + w_{smp}^2 + w_{IGM}^2)}/(1+z)$ is a real quantity for all the resolved FRBs in Table 1.

While w_{IGM} from model 1 is based on the assumption that the nature of IGM turbulence is similar to that of the

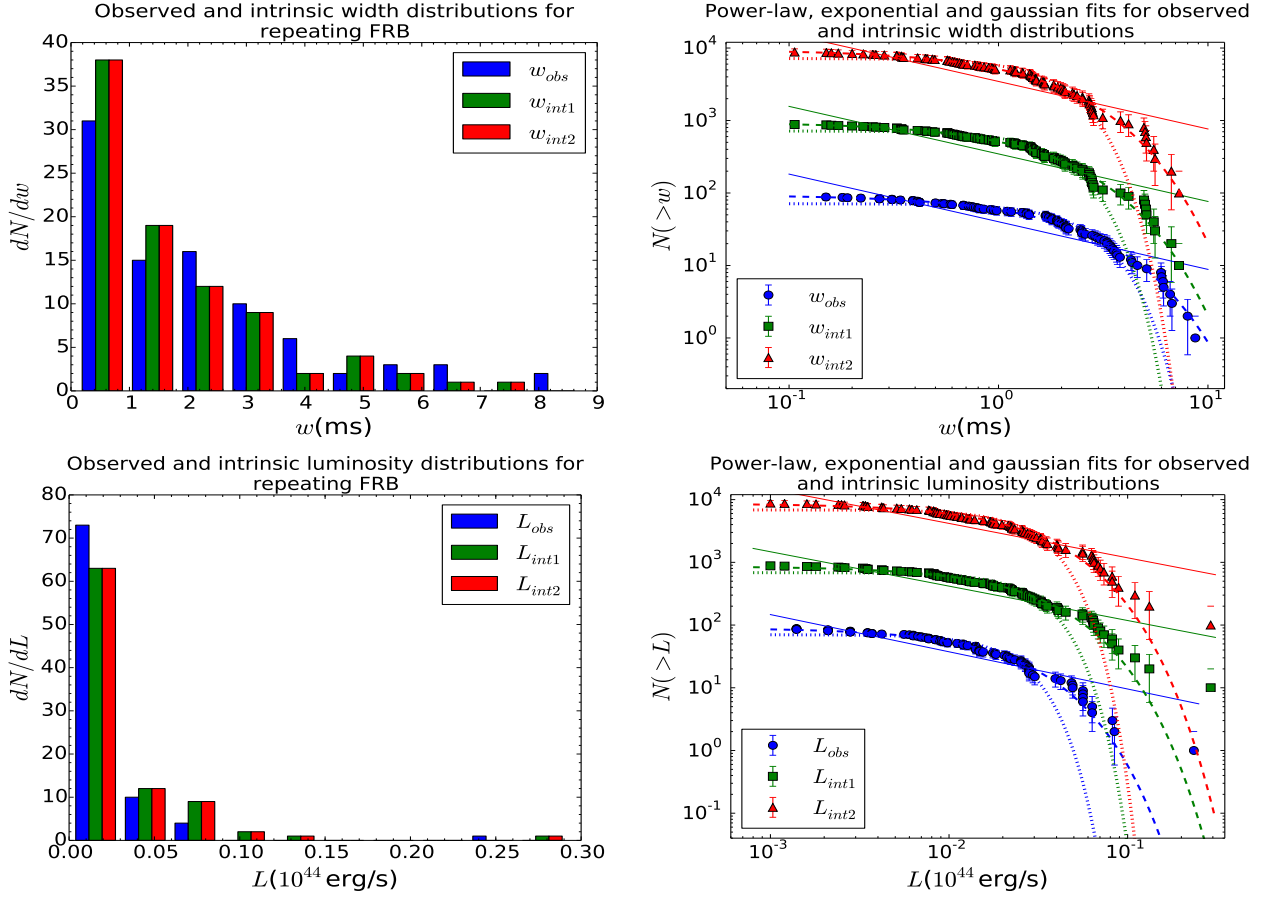


Figure 2. Pulse width and luminosity distributions for repeating bursts: *Top-left panel:* Histograms for widths w_{obs} , w_{int1} and w_{int2} , *Top-right panel:* Chi-squared fits for cumulative distributions of w_{obs} , w_{int1} and w_{int2} , *Bottom-left panel:* Histograms of luminosities L_{obs} , L_{int1} and L_{int2} , *Bottom-right panel:* Chi-squared fits for cumulative distributions of L_{obs} , L_{int1} and L_{int2} . The index 1/2 for the burst parameters denotes scattering model 1/2. The burst parameters for the repeating FRB 121102 are obtained from Spitler et al. (2016), Scholz et al. (2016), Scholz et al. (2017), Law et al. (2017), Hardy et al. (2017), Michilli et al. (2018), Gajjar et al. (2018) and Spitler et al. (2018). The functional forms used for the chi-squared fits of the cumulative distributions are power-law, exponential and gaussian (see Table A3).

Galactic ISM and can be estimated with an observationally established empirical fit, w_{IGM} from model 2 is based on a completely theoretical model for IGM turbulence which has not been observationally verified. Previous FRB population studies (Bera et al. 2016; Caleb et al. 2016) have used $w_{ISM} - DM$ relation for pulsars in the MW ISM from Bhat et al. (2004) in order to estimate the IGM and ISM scatter broadening widths. However, it has already been shown by Hassall et al. (2013) and Lorimer et al. (2013) that the scatter broadening of known FRBs is significantly smaller compared to that estimated from the Bhat et al. (2004) model. The pulse scattering width estimated from the Bhat et al. (2004) model increases considerably beyond $z \sim 0.5$ (see Figure 1 of Bera et al. 2016) and typically exceeds the observed pulse widths for the known FRBs at high redshifts (see Table 1). For $DM_{host/MW} \lesssim 100 \text{ pc cm}^{-3} \ll DM_{IGM}$, $w_{ISM,host/MW}$ obtained from equation (4) is considerably smaller compared to w_{IGM} and other width components in equation (3). The values of all the observed burst and telescope parameters in equations (1-6) are obtained from the FRB catalogue.

2.2 Luminosity and energy estimates

As the width of a radio pulse gets broadened by scattering in the turbulent plasma, the pulse is smeared across a longer time interval, thereby reducing its peak flux density. The fluence \mathcal{F}_{obs} , proportional to the total emitted energy of the pulse, is assumed to be unaffected by the scatter broadening for each burst. Once w_{int} for a given FRB is obtained from equation (3), the corresponding intrinsic peak flux density can be estimated from the fluence as $S_{peak,int} = \mathcal{F}_{obs}/w_{int}$. For a power-law energy distribution of the FRB source, the bolometric luminosity and energy for the burst are given by (Lorimer et al. 2013),

$$L = S_{peak} \times \frac{4\pi D^2(z)(\nu_{max}^{\alpha+1} - \nu_{min}^{\alpha+1})}{(1+z)^{\alpha-1}} \left(\frac{\nu_2 - \nu_1}{\nu_2^{\alpha+1} - \nu_1^{\alpha+1}} \right)$$

$$E = \mathcal{F}_{obs} \times \frac{4\pi D^2(z)(\nu_{max}^{\alpha+1} - \nu_{min}^{\alpha+1})}{(1+z)^{\alpha-1}} \left(\frac{\nu_2 - \nu_1}{\nu_2^{\alpha+1} - \nu_1^{\alpha+1}} \right) \quad (7)$$

where $\nu'_{min/max}$ is the minimum/maximum emission frequency of the FRB source, α is the spectral index and $\nu_{1/2}$ is the lowest/highest frequency in the observing band of the telescope. In order to evaluate the intrinsic lumi-

osity and energy distributions for the observed bursts, we assume a flat energy spectrum ($\alpha \approx 0$) to obtain: $L_{int} = 4\pi S_{peak,int} D^2(z)(\nu'_{max} - \nu'_{min})(1+z)$ and $E_{obs} = 4\pi \mathcal{F}_{obs} D^2(z)(\nu'_{max} - \nu'_{min})(1+z)$. Here we use $\nu'_{min} = 600$ MHz and $\nu'_{max} = 8$ GHz that are consistent with the current observed FRB population (FRB catalogue). The assumption of a flat energy spectrum is reasonable as the FRB emission spectrum is poorly constrained at present with the spectral indices varying within a wide range.

The left-half panels in Figure 1 show the histograms for the distributions of pulse width and luminosity of the 23 non-repeating bursts from Table 1, while the right-half panels show three functional fits for the cumulative distributions of the corresponding quantities. We obtain chi-squared fits for the cumulative distributions of the non-repeating burst parameters using three different functional forms: power-law, exponential and gaussian with zero mean, where the error for each data point is quantified with Poisson fluctuations. We find that w_{int} for most bursts is a factor of $\sim 2-3$ smaller compared to w_{obs} and is within a relatively broad range of $\sim 0.3-10$ ms. While most of the bursts have $w_{int} \lesssim 5$ ms, there is considerable spread in the width values suggesting that they are not peaked around $w_{int} \approx 1$ ms as assumed for previous MC simulations (Bera et al. 2016; Caleb et al. 2016).

We find that the cumulative distribution of w_{int} for non-repeating bursts is best fitted with an exponential distribution, with a cutoff around $w_{int} \sim 2$ ms that is about half of the w_{obs} exponential cutoff. L_{int} varies by almost four orders of magnitude from $\sim 10^{43}$ erg/s to $\sim 10^{47}$ erg/s with a peak luminosity around $\sim 6 \times 10^{44}$ erg/s. As the inferred L_{int} values of the observed non-repeating bursts vary within a wide range, FRBs are significantly unlikely to be standard candles. We find that the cumulative distribution of L_{int} is best fitted with an exponential distribution for the non-repeating bursts, with a L_{int} cutoff around $\sim 2 \times 10^{45}$ erg/s that is roughly twice of the exponential cutoff for L_{obs} . Furthermore, there is no significant difference in the width and luminosity distribution fit parameters obtained by changing the scattering models.

The left-half panels in Figure 2 show the histograms for the width and luminosity distributions of the known sub-bursts from the repeating FRB 121102. The right-half panels show the chi-squared fits (with the same functional forms as the non-repeating bursts) for the cumulative width and luminosity distributions. Even though the average w_{int} for repeating burst is smaller compared to that for the non-repeating bursts, it still varies by almost two orders of magnitude from $\sim 0.1-8$ ms with most bursts having $w_{int} \lesssim 3$ ms. The fractional pulse broadening $\Delta w_{int}/w_{int} = (w_{obs} - w_{int})/w_{int}$ for the repeater is also found to be smaller compared to the non-repeating bursts, which is expected due to its smaller distance, and thereby lesser scatter and dispersion broadening. The cumulative w_{int} distribution is best fitted with an exponential distribution with a cutoff $w_{int} \sim 1.6$ ms that is slightly smaller than the corresponding cutoff for $w_{obs} \sim 2.1$ ms. The luminosity varies in a considerably smaller range, $L_{int} \sim 10^{41} - 10^{43}$ erg/s, compared to the non-repeaters. We find that the cumulative L_{int} distribution is best fitted with an exponential distribution, with a cutoff $L_{int} \sim 2.7 \times 10^{42}$ erg/s that is slightly larger compared to the L_{obs} cutoff. Similar to the non-repeating

bursts, the difference between the scattering models is almost negligible.

2.3 Burst parameter correlation and width components

Once the burst parameters are estimated from the FRB observables, we can study the correlation between different parameters and the burst distance/energy for the non-repeating/repeating FRBs. We show the dependence of S_{peak} , DM and L on z for the non-repeating bursts in the top-left, top-right and bottom-left panels of Figure 3. We find that both the observed and intrinsic S_{peak} of these events have no apparent correlation with the inferred distances. However, the relative scatter in the flux values for a given distance is considerably larger for intermediate $z \sim 1$. While the IGM contribution to the DM is found to be comparable to the host galaxy contribution for small $z \approx 0.2$, $DM_{IGM}/DM_{host} \gtrsim 10$ for larger $z \gtrsim 0.6$. As most of the currently detected bursts have $z \gtrsim 0.6$, small variations in DM_{host} is not expected to significantly affect $DM_{Ex} = DM_{host} + DM_{IGM}$, provided that the typical host galaxy properties are not very different from that of the MW. Furthermore, we only consider FRBs with $DM_{tot} \geq 500$ pc cm $^{-3}$ to minimize the error in the inferred z due to the assumptions about the host galaxy properties. The burst luminosities increase on an average with an increase in the burst distance, which is expected as S_{peak} for FRBs is almost independent of z . Moreover, the bursts with higher L_{int} are easier to detect from larger distances compared to dimmer FRBs, for a given telescope sensitivity. Due to the apparent positive correlation of the burst luminosities with their inferred distances, FRBs are not expected to be standard candles as previously expected. In the bottom-right panel of Figure 3, the dependence of S_{peak} on E_{obs} is shown for the reported sub-bursts of repeating FRB 121102. We find that the more energetic sub-bursts have a larger value of S_{peak} on average, which is reasonable as brighter bursts detected from a given distance are expected to emit more energy.

The scatter broadening width for a given FRB source can be written as, $w_{sc} = [w_{ISM,MW}^2 + w_{ISM,host}^2(1+z)^2 + w_{IGM}^2]^{0.5}$. For non-repeating FRBs, we show the variation of the observed width components w_{DM} , w_{sc} and w_{int} with distance in the top-left panel of Figure 4, while the variation of the scattering width components $w_{ISM,host}$, $w_{ISM,MW}$ and w_{IGM} with distance are shown in the top-right panel of Figure 4. The ISM broadening contributions are found to be very small with $w_{ISM,MW} \lesssim 10^{-3}$ ms and $w_{ISM,host} \lesssim 10^{-6}$ ms, which is expected as the ISM contribution is suppressed relative to the IGM contribution by the geometrical factor $4f(1-f) \sim 10^{-4}$. While the width broadening due to IGM turbulence is larger at least by an order of magnitude for scattering model 2 at smaller redshifts $z \lesssim 1$, the IGM contributions for both scattering models are roughly equal for $z \gtrsim 2$ as w_{IGM} increases faster with distance for model 1. The dispersive smearing w_{DM} is approximately of the same order of magnitude as w_{obs} and w_{int} for a given FRB, with 10^{-1} ms $\lesssim w_{DM} \lesssim 10^1$ ms for all bursts. The smallest contribution to the pulse width broadening is from scattering with $w_{sc} \lesssim 1$ ms for almost all bursts. As $w_{obs} \sim w_{DM} \gg w_{sc}$ for most FRBs, w_{DM}

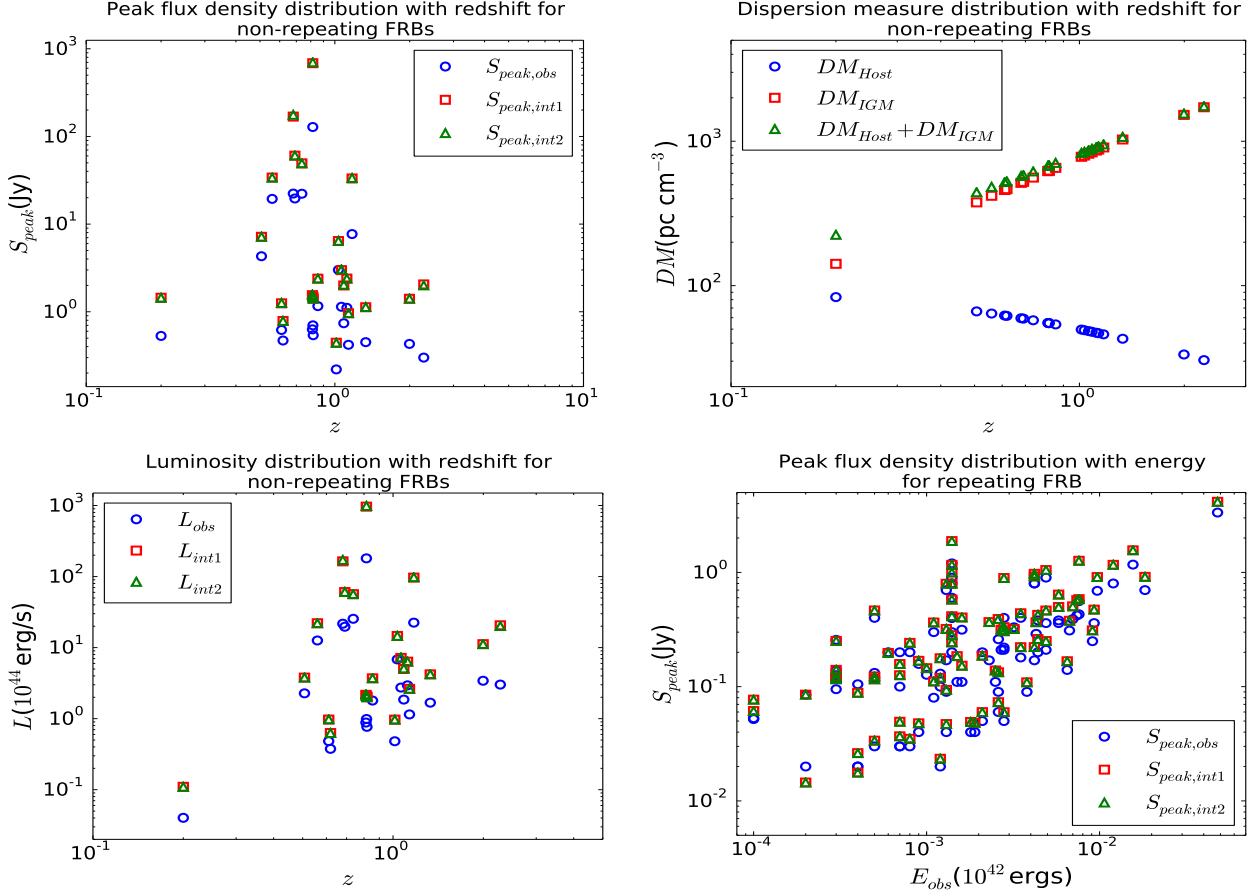


Figure 3. Variation of burst parameters with distance for non-repeating bursts and with energy for repeating FRB: Top-left panel: Dependence of peak flux densities S_{peak} on distance for non-repeating FRBs, Top-right panel: Dependence of dispersion measure DM_{tot} on distance for non-repeating FRBs, Bottom-left panel: Dependence of luminosities L on distance for non-repeating FRBs, Bottom-right panel: Dependence of peak flux densities S_{peak} on burst energy for FRB 121102.

is the dominant contribution to the temporal broadening. Even though the intrinsic pulse width varies considerably with $10^{-1} \text{ ms} \lesssim w_{int} \lesssim 10 \text{ ms}$, the two scattering models are essentially indistinguishable due to the small scatter broadening contributions with $w_{int,1} \approx w_{int,2}$.

The bottom-left panel of Figure 4 shows the variation of w_{obs} components with E_{obs} , while the bottom-right panel shows the variation of w_{sc} components with the emitted energy for the sub-bursts of FRB 121102. We find that the ISM broadening contributions from both host galaxy and MW are very small with $w_{ISM,host/MW} \lesssim 10^{-4} \text{ ms}$ for all sub-bursts. As the redshift $z \approx 0.19273$ is relatively small for FRB 121102, the width broadening due to IGM turbulence is much more significant for scattering model 2 relative to model 1. The dispersive smearing is found to be smaller compared to most non-repeating FRBs with $10^{-1} \text{ ms} \lesssim w_{DM} \lesssim 1 \text{ ms}$. While w_{obs} and w_{int} are approximately of the same order of magnitude, w_{DM} is about one order of magnitude smaller. We find that scatter broadening $w_{sc} \lesssim 2 \times 10^{-2} \text{ ms}$ is the smallest contribution to the width broadening. Even though w_{DM} is the dominant contribution to the pulse broadening with $w_{obs} > w_{DM} \gg w_{sc}$, w_{DM} for FRB 121102 sub-bursts are considerably smaller compared to that for the non-repeating FRBs due to the relatively small DM_{tot} for FRB 121102. The intrinsic width varies

considerably within $1 \text{ ms} \lesssim w_{int} \lesssim 10 \text{ ms}$ with $w_{int} \approx w_{obs}$, implying that a considerable fraction of w_{obs} for FRB 121102 is from w_{int} and not due to the dispersive smearing or scatter broadening of the pulse. Although $w_{sc1} \ll w_{sc2}$, the scattering models are still indistinguishable with $w_{int,1} \approx w_{int,2}$ due to the minimal IGM and ISM scatter broadening contributions.

For both non-repeating bursts and FRB 121102, we find that most of the pulse temporal broadening is due to dispersive smearing and not IGM or ISM scattering. The contribution from w_{DM} to the width broadening is found to be considerably larger for the non-repeating FRBs in comparison to the FRB 121102 sub-bursts, which is expected due to the larger DM_{tot} values for the non-repeating FRBs. The IGM scatter broadening is the dominant contribution to w_{sc} for both classes of FRBs while the w_{ISM} contributions are significantly smaller due to the geometrical lever-arm effect. The intrinsic width for both FRB classes is found to be largely scattering model-independent. Moreover, there is a considerable spread in the w_{int} values within a range of $\sim 10 \text{ ms}/\sim 8 \text{ ms}$ for the non-repeating/repeating bursts with most FRBs having $w_{int} \lesssim 5 \text{ ms}/w_{int} \lesssim 3 \text{ ms}$. We estimate the average relative broadening of the intrinsic width, $\Delta w_{int}/w_{int} = (w_{obs} - w_{int})/w_{int}$, to be $\sim 150\%/\sim 20\%$ for the non-repeating/repeating FRBs.

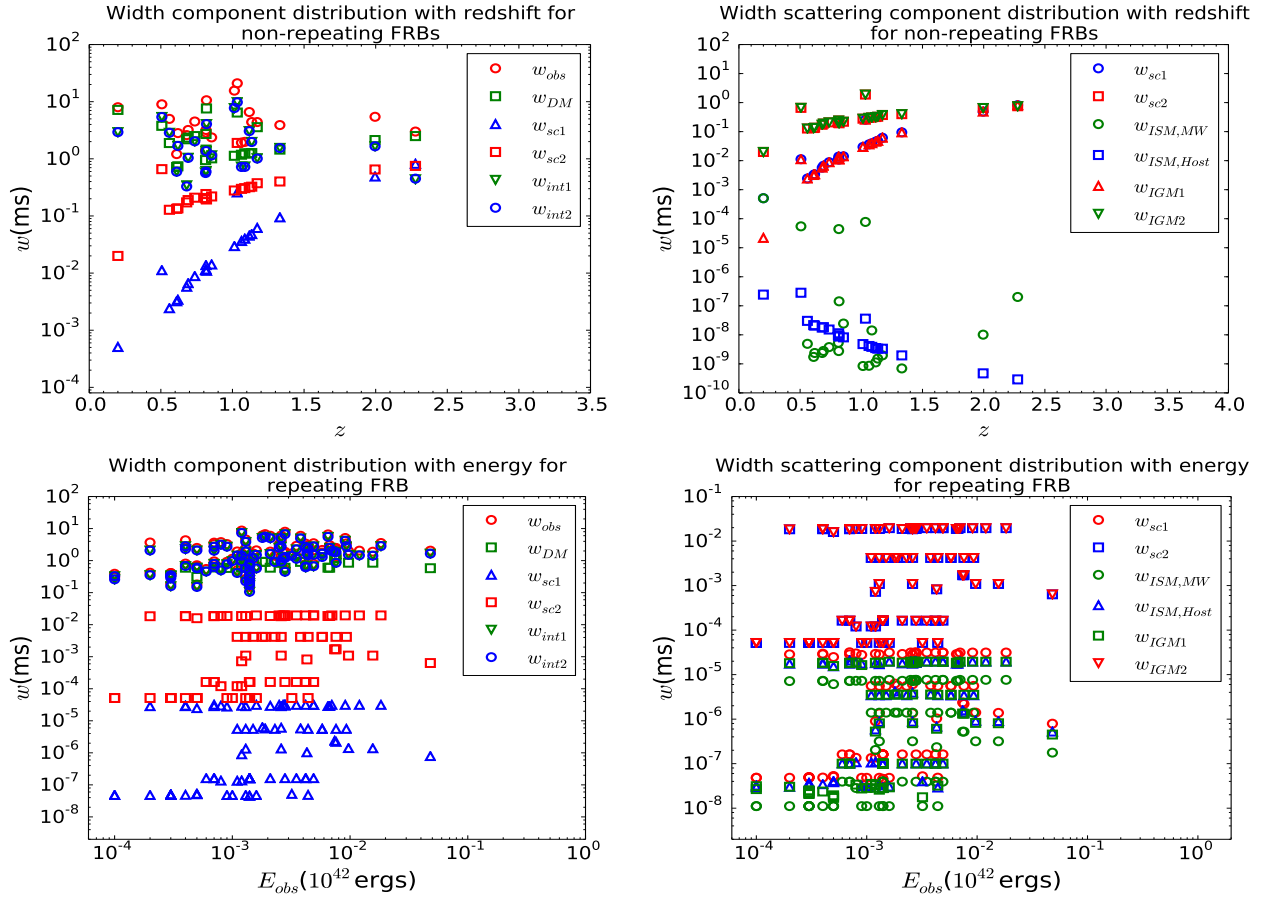


Figure 4. Variation of pulse width components for non-repeating FRBs and repeating FRB 121102: Top-left panel: Variation of w_{obs} components - w_{DM} , w_{sc} and w_{int} , with distance for non-repeating FRBs, Top-right panel: Variation of w_{sc} components - $w_{ISM,host}$, $w_{ISM,MW}$ and w_{IGM} , with distance for non-repeating FRBs, Bottom-left panel: Variation of w_{obs} components with burst energy for FRB 121102 sub-bursts, Bottom-right panel: Variation of w_{sc} components with burst energy for FRB 121102 sub-bursts.

Table 2. System parameters for the Parkes multibeam (MB) receiver are obtained from Thornton (2013) and those for the Arecibo L-band feed array (ALFA) are obtained from Spitler et al. (2014).

Parameter	Parkes MB	Arecibo ALFA
Digitization factor (β)	1.07	1.16
System temperature (T_{sys})	30	30
Central frequency in MHz (ν_0)	1352	1375
Frequency bandwidth in MHz (ν_{bw})	338	323
Channel bandwidth in MHz ($\Delta\nu_0$)	0.390	0.336
Sampling width in ms (w_{samp})	0.0640	0.0655

3 MONTE CARLO SIMULATIONS

In the previous section, we developed a formalism in order to estimate the intrinsic properties of the FRBs such as w_{int} , $S_{peak,int}$, L_{int} and E_{obs} , from the observables for both non-repeating and repeating bursts. Here we describe our MC code with which we constrain the various properties of the FRB source, its host galaxy and the intervening turbulent plasma from the observed properties of the reported FRBs. We first discuss the initial parameters and distributions used

in the MC code. Next, we briefly describe the algorithm of our MC code.

3.1 Input parameters

The input parameters used for our MC simulations are:

- *Burst type:* We categorise all FRBs into two different classes of bursts: non-repeating and repeating FRBs. We model the population of the non-repeating/repeating

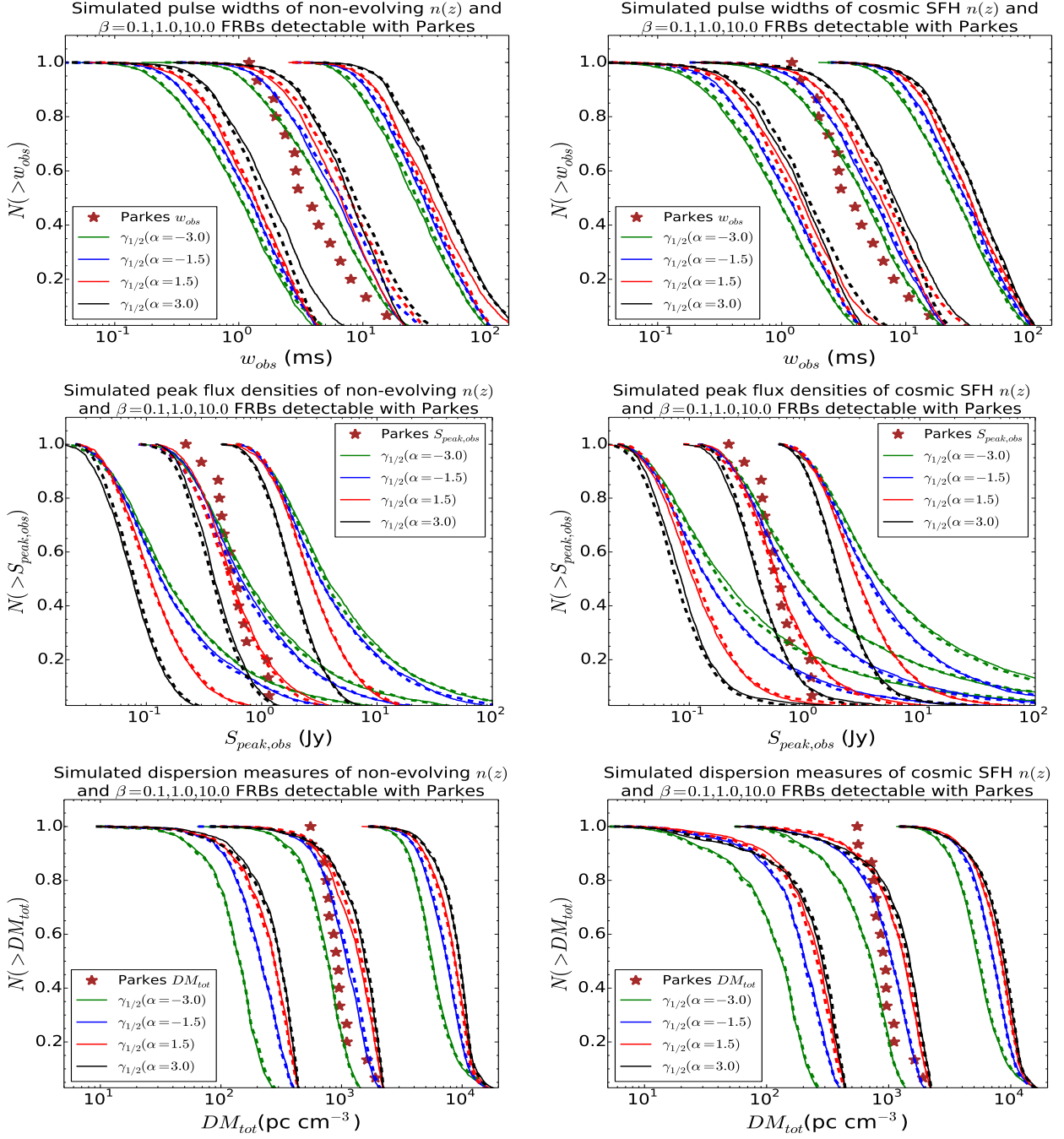


Figure 5. Comparison of w_{obs} , $S_{peak,obs}$ and DM_{tot} for simulated NE (left-half panels) and SFH (right-half panels) FRBs with non-repeating FRBs detected by Parkes: In each panel, the MC simulation results are shown for DM_{host} parameter $\beta = 0.1, 1.0, 10.0$, spectral index $\alpha = -3.0, -1.5, 1.5, 3.0$ and both scattering models. The values for the burst parameters are scaled from their actual values by a factor of 0.2/5.0 for $\beta = 0.1/10.0$ to avoid overlap. *Top-left panel:* Simulation results for w_{obs} of NE FRBs, *Top-right panel:* Simulation results for w_{obs} of SFH FRBs, *Center-left panel:* Simulation results for $S_{peak,obs}$ of NE FRBs, *Center-right panel:* Simulation results for $S_{peak,obs}$ of SFH FRBs, *Bottom-left panel:* Simulation results for DM_{tot} of NE FRBs, *Bottom-right panel:* Simulation results for DM_{tot} of SFH FRBs. The scattering model 1/2 is denoted by the dashed/solid lines and the index 1/2 for the KS values.

FRBs found at the Parkes MB/Arecibo ALFA (see Table 2 for the system parameters of these surveys). Parkes MB/Arecibo ALFA has 13/7 beams with different beam center gains G_{beam} and beam radii r_{beam} . For Parkes MB, $r_{beam} = 7.0'$ (7.05') [7.25'] and $G_{beam} = 0.731$ (0.690) [0.581] K Jy $^{-1}$ for beam 1 (2-7) [8-13], while Arecibo ALFA has $r_{beam} = 3.35'$ (3.35') and

$$G_{beam} = 10.4 \text{ (8.2) K Jy}^{-1} \text{ for beam 1 (2-7).}$$

- *Scattering model:* To determine the scatter broadening of the intrinsic pulse width for each FRB due to propagation through the turbulent ISM and IGM, we consider either scattering model 1 or model 2 (see Section 2.1).

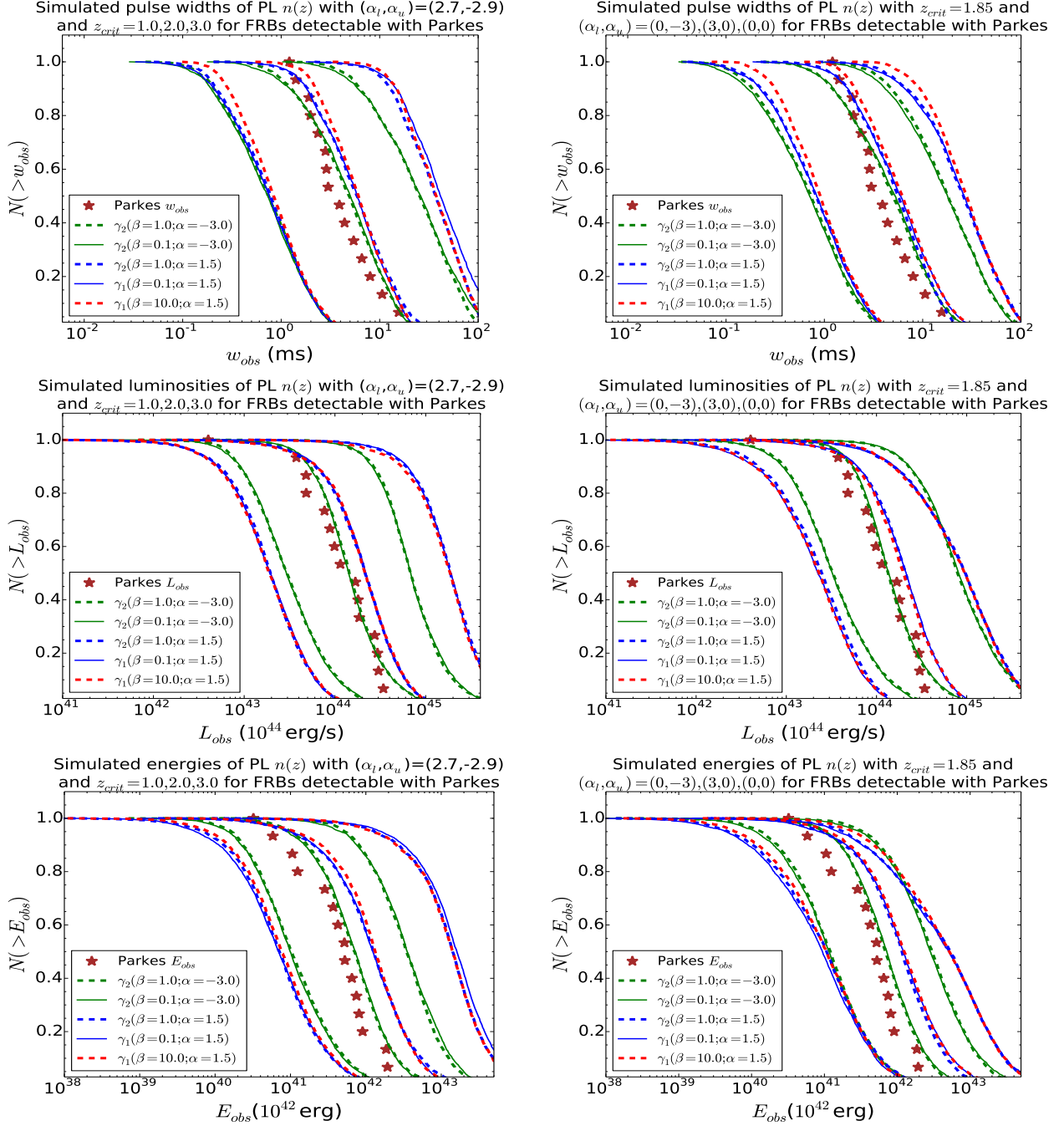


Figure 6. Comparison of non-repeating FRBs detected by Parkes and simulated w_{obs} , L_{obs} and E_{obs} for PL FRB population with varying z_{crit} (left-half panels) or varying (α_l, α_u) (right-half panels): The MC simulation results are shown for the six cases described in Section 4.2 with the KS subscripts denoting the scattering model. The FRB parameter values are scaled by a factor 0.2/5.0 for $z_{crit} = 1.0/3.0$ in the left-half panels, while the corresponding values are scaled by 0.2/5.0 for $(\alpha_l, \alpha_u) = (0, -3)/(0, 0)$ in the right-half panels to avoid overlap. *Top-left panel:* Simulated w_{obs} for fixed $(\alpha_l, \alpha_u) = (2.7, -2.9)$ and varying $z_{crit} = 1.0, 2.0, 3.0$ for FRBs detectable with Parkes, *Top-right panel:* Simulated w_{obs} for fixed $z_{crit} = 1.85$ and varying $(\alpha_l, \alpha_u) = (0, -3), (3, 0), (0, 0)$, *Center-left panel:* Simulated L_{obs} for fixed (α_l, α_u) and varying z_{crit} , *Center-right panel:* Simulated L_{obs} for fixed z_{crit} and varying (α_l, α_u) , *Bottom-left panel:* Simulated E_{obs} for fixed (α_l, α_u) and varying z_{crit} , *Bottom-right panel:* Simulated E_{obs} for fixed z_{crit} and varying (α_l, α_u) .

- *FRB source spatial density $n(z)$:* In order to estimate the number of FRB sources in a given comoving volume, we consider three different spatial density distributions:

(i) *Non-evolving (NE) population:* The number of FRB progenitors increases linearly with the comoving vol-

ume for a non-evolving population. From Table 1, we know that the maximum inferred redshift value for the reported FRBs is $z \approx 2.3$. We generate FRBs upto a maximum redshift $z_{max} = 3.0$, corresponding to a maximum comoving volume $V_{c,max} \approx 1286 \text{ Gpc}^3$ for typical cosmological parameters. The comoving distances

to the FRBs are obtained as $D_c = (3\zeta_1 V_{c,max}/4\pi)^{1/3}$, where ζ_1 is a uniform random number between 0 and 1. The associated z is then obtained by inverting $D(z) = (8.49 \text{ Gpc}) \int_0^z [(1+z')^3 + 2.7]^{-0.5} dz'$.

- (ii) *Tracking cosmic star formation history (SFH)*: As the majority of the FRB progenitor models suggested (including both cataclysmic and non-cataclysmic scenarios) involve young neutron stars, the spatial distribution of FRBs is expected to track the cosmic SFH. Furthermore, few reported FRBs have inferred distances exceeding $z \approx 2.0$, in which case the FRB spatial density can be significantly different compared to a NE population. We consider the cosmic SFH functional fit suggested by [Madau & Dickinson \(2014\)](#),

$$\psi(z) = (0.015 \text{ M}_\odot \text{ yr}^{-1} \text{ Mpc}^{-3}) \frac{(1+z)^{2.7}}{1 + [(1+z)/2.9]^{5.6}} \quad (8)$$

The FRB redshifts are generated by inverting $\zeta_2 = \int_0^z \psi(z') dz' / \int_0^3 \psi(z') dz'$, where ζ_2 is a uniform random number between 0 and 1. We then obtain $z = 12.05\zeta_2 - 57.16\zeta_2^2 + 167.97\zeta_2^3 - 259.28\zeta_2^4 + 199.04\zeta_2^5 - 59.63\zeta_2^6$.

- (iii) *Power-law (PL) distribution*: We also consider a broken power-law FRB spatial density given by,

$$n(z) = n_0 \begin{cases} (1+z)^{\alpha_l}, & z_{min} \leq z < z_{crit} \\ (1+z)^{\alpha_u}, & z_{crit} \leq z \leq z_{max} \end{cases} \quad (9)$$

where n_0 is a constant, α_l/α_u is the lower/upper power-law index, z_{min}/z_{max} is the minimum/maximum redshift and z_{crit} is the redshift at which $n(z)$ peaks. We try to constrain the distribution parameters α_l , α_u and z_{crit} from the observed FRB population. From the cosmic SFH fit (equation 8), we have $\alpha_l \approx 2.7$ at low z , $\alpha_u \approx -2.9$ at high z and $z_{crit} \approx 1.85$ from the peak of the distribution. We use $z_{min} = 0$ and $z_{max} = 3.0$ to generate the FRB redshifts from the power-law $n(z)$ distribution.

- *β -parameter for DM_{host}* : As opposed to a constant DM_{host} contribution along all lines of sight, we assume that the free electron density distribution in the host galaxy is similar to that of the MW and can be obtained using the NE2001 model. We estimate the DM contribution due to the host galaxy ISM along the FRB source line of sight as, $DM_{host} = \beta DM_{NE2001}$, where β is the parameter that accounts for the size of the FRB source host galaxy relative to the MW and DM_{NE2001} is the DM value predicted by the NE2001 model. In this work, we consider $\beta = 0.1, 1.0$ and 10.0 for the non-repeating FRBs. For the repeating FRB 121102, we use $DM_{MW} = 188 \text{ pc cm}^{-3}$ and $DM_{host} = 281 \text{ pc cm}^{-3}$ for all generated FRBs.

- *FRB energy density spectral index α* : Instead of using a flat FRB energy spectrum, we assume that the FRB energy spectrum can be modelled using a power-law, $E_{\nu'} = k\nu'^\alpha$, where ν' is the frequency in the source frame and α is the spectral index. The FRB bolometric luminosity and energy are then given by equation (7). Even though the coherent emission mechanism for FRBs suggests a negative spectral index, the spectral indices for some of the reported bursts

vary within a wide range. For completeness, here we consider $\alpha = -3.0, -1.5, 1.5$ and 3.0 .

3.2 MC code algorithm

At the start of the simulation, we select a specific scattering model and burst type for the FRB events to be generated. We then draw the intrinsic pulse width w_{int} and luminosity L_{int} of the first event from the corresponding best fit chi-squared distributions (Tables A2 and A3) and compute the burst energy $E_{int} = w_{int} L_{int}$. Next, we draw $D(z)$ for the burst and evaluate the corresponding z for the chosen FRB spatial density model $n(z)$. Once the distance to the FRB is known, we further estimate $DM_{IGM}(z)$ and $w_{IGM}(z)$ for the scattering model selected. We then draw a random line of sight in the MW and get DM_{MW} from the NE2001 model. For the host galaxy ISM contribution, we choose a random line of sight in the host galaxy to evaluate $DM_{host} = \beta DM_{NE2001}$ for the β value selected. Once the DM_{MW} and DM_{host} contributions are known, we obtain the corresponding width broadening components $w_{ISM,MW}$ and $w_{ISM,host}$. We include the IGM contribution to the DM to estimate DM_{tot} and the pulse dispersive smearing w_{DM} . The observed pulse width w_{obs} is obtained by adding w_{samp} to the previously estimated width components (see equation 3).

For a power-law FRB energy density with spectral index α chosen earlier, the peak flux density at the beam center $S_{peak,bc}$ can be obtained from L_{int} for an observation in the frequency band between $\nu_1 = \nu_0 - (1/2)\nu_{bw}$ and $\nu_2 = \nu_0 + (1/2)\nu_{bw}$ as

$$S_{peak,bc} = \frac{L_{int}(1+z)^{\alpha-1}}{4\pi D(z)^2 (\nu_{max}'^{\alpha+1} - \nu_{min}'^{\alpha+1})} \left(\frac{\nu_2^{\alpha+1} - \nu_1^{\alpha+1}}{\nu_2 - \nu_1} \right) \quad (10)$$

We assume FRB coherent emission to be in the frequency range between $\nu_{min}' = 600 \text{ MHz}$ and $\nu_{max}' = 8 \text{ GHz}$, in agreement with the current observations. However, the observed flux $S_{peak,obs}$ can be significantly smaller compared to $S_{peak,bc}$ due to the finite telescope beam size and for a Gaussian beam profile is given by

$$S_{peak,obs} = S_{peak,bc} \exp \left[-(2 \ln 2) \frac{r'^2}{r_{beam}^2} \right] \quad (11)$$

While the probability of a particular beam detecting the FRB event is proportional to its area $\sim \pi r_{beam}^2$, the radial distance r' from the beam center is chosen randomly. For pulses detected in single-pulse searches, the search trial width w_{trial} has to be closest to the observed pulse width w_{obs} . In our simulation, we generate w_{trial} in powers of two starting from w_{samp} in order to find w_{trial} nearest to w_{obs} . Once w_{trial} is determined, the signal-to-noise ratio S/N for optimal detection is obtained from $S_{peak,obs}$ and the other telescope parameters as

$$\frac{S}{N} = \frac{S_{peak,obs}}{\beta T_{sys}} G_{beam} \sqrt{2\nu_{bw} w_{trial}} \quad (12)$$

The FRB event is detected only if $S/N \geq 9$ (5) for Parkes MB (Arecibo ALFA) and the simulation continues with the aforementioned algorithm until $N_{det} = 3000$ events have been detected. From $S_{peak,obs}$ of a given FRB, we further obtain the observed fluence $\mathcal{F}_{obs} = S_{peak,obs} w_{obs}$, luminosity $L_{obs} = 4\pi D(z)^2 (1+z) S_{peak,obs} (\nu_{max}' - \nu_{min}')$

and energy $E_{obs} = 4\pi D(z)^2(1+z)\mathcal{F}_{peak,obs}(\nu'_{max} - \nu'_{min})$. The observed ($S_{peak,obs}$, \mathcal{F}_{obs} , DM_{tot} , w_{obs}) and inferred (z , L_{obs} , E_{obs}) properties for every detected burst are stored for comparison with the observed FRB population in order to constrain the input parameters.

4 SIMULATION RESULTS AND PARAMETRIC CONSTRAINTS

In the previous section, we described the MC code algorithm and discussed the input parameters for our code. Here we present the simulation results for the non-repeating FRBs and further compare them with the current observations in order to constrain the model parameters of the FRB population. We first discuss the simulation results of the NE and SFH $n(z)$ distributions for non-repeating FRBs that are detectable with Parkes to identify the parametric spaces (β, α) where the KS value γ is maximised for a given choice of the scattering model and $n(z)$ distribution. Then, we specifically consider the cases where γ is maximised to further constrain the parameters of the PL $n(z)$ distribution and identify ($\alpha_l, \alpha_u, z_{crit}$) favored by the observations.

4.1 NE and SFH FRB spatial densities

We show the results for the simulated w_{obs} , $S_{peak,obs}$ and DM_{tot} distributions of the non-repeating FRBs and compare them with the data from Parkes at $\nu_{obs} = 1.4$ GHz in Figure 5. These simulations are performed for NE and SFH $n(z)$ distributions with DM_{host} in the range $\beta \sim 0.1 - 10.0$ and the energy spectral index within range $\alpha \sim -3.0$ to 3.0. We consider both scattering models for the MC simulations even though their relative difference is not found to be significant for the parametric space considered (see Section 2). We consider w_{obs} and $S_{peak,obs}$ to be the independent parameters among (w_{obs} , $S_{peak,obs}$, \mathcal{F}_{obs}) in addition to DM_{tot} to evaluate the equivalent KS value $\gamma_{eq} = \sqrt{\gamma_{w_{obs}}^2 + \gamma_{S_{peak,obs}}^2 + \gamma_{DM_{tot}}^2}$ in each case.

We find that for both NE and SFH populations of the FRBs, the observed w_{obs} from Parkes are in better agreement with the simulated w_{obs} for a relatively small DM_{host} contribution corresponding to $\beta \sim 0.1 - 1.0$ as opposed to $\beta \gtrsim 10.0$. Moreover, the observed w_{obs} distribution suggests a large negative spectral index α for the FRB energies as $\gamma_{w_{obs}}$ gradually decreases as α increases for both $n(z)$ distributions. In case of $S_{peak,obs}$, we find that the DM_{host} contribution does not significantly affect the observed distribution for either of the FRB population densities. However, the observed $S_{peak,obs}$ from Parkes can be better explained for a shallower FRB energy spectrum with $\gamma_{S_{peak,obs}}(\alpha = 1.5) \gg \gamma_{S_{peak,obs}}(\alpha = -1.5) > \gamma_{S_{peak,obs}}(\alpha = \pm 3.0)$ for both $n(z)$ considered. For both $n(z)$ distributions used here, $DM_{host} \lesssim DM_{MW}$ is clearly favored from the DM_{tot} detected at Parkes with $\gamma_{DM_{tot}}(\beta \sim 0.1 - 1.0) \gg \gamma_{DM_{tot}}(\beta \sim 10.0)$. The observed DM_{tot} values at Parkes are expected to arise from a relatively shallow FRB energy density distribution with $\alpha \approx -1.5$ for both FRB $n(z)$.

While the scattering models for IGM and ISM turbulence cannot be significantly differentiated using the observed non-repeating FRB population at present, model 2 is found to be in slightly better agreement with the Parkes data. From the simulated FRB parameters and the Parkes data, we find that the host DM contribution is likely to be smaller or comparable to the MW contribution with the likelihood order $\beta = 1.0 \approx \beta = 0.1 > \beta = 10.0$. Furthermore, a larger negative value of α is favored by the FRB observations in general with the order $\alpha = -3.0 > \alpha = 1.5 \gtrsim \alpha = -1.5 \gg \alpha = 3.0$. While the non-repeating FRB population observed with Parkes that is considered here does not clearly differentiate between the FRB $n(z)$ distributions, we find the SFH FRB spatial density to be more likely. It should be noted that NE and SFH $n(z)$ have similar redshift distribution for FRBs upto $z \approx 2.0$, where most of the FRBs are generated in the MC simulations and also observed.

4.2 PL FRB spatial density

From the top-half of Table C1, the five cases with either NE or SFH $n(z)$ for which γ_{eq} is maximised and $\gamma_{eq} \geq 0.2$ for a given choice of β , α and the scattering model can be identified as:

- (1) $\beta = 1.0$ and $\alpha = -3.0$ for scattering model 2
- (2) $\beta = 0.1$ and $\alpha = -3.0$ for scattering model 2
- (3) $\beta = 1.0$ and $\alpha = 1.5$ for scattering model 2
- (4) $\beta = 0.1$ and $\alpha = 1.5$ for scattering model 1
- (5) $\beta = 10.0$ and $\alpha = 1.5$ for scattering model 1

We show the simulated w_{obs} , L_{obs} and E_{obs} distributions corresponding to these cases for comparison with the observed non-repeating FRB population detected by Parkes at $\nu_{obs} = 1.4$ GHz in Figure 6. In order to constrain the parameters ($\alpha_l, \alpha_u, z_{crit}$) of the PL $n(z)$ distribution, we perform the MC simulations with either varying z_{crit} or varying (α_l, α_u) for each of these cases listed above. We consider $z_{crit} = 1.0, 2.0, 3.0$ for fixed (α_l, α_u) = (2.7, -2.9), where the values for the PL indices are motivated from the SFH distribution at asymptotically low and high redshifts. For the fixed z_{crit} case, we consider (α_l, α_u) = (0, -3), (3, 0), (0, 0) and the value of $z_{crit} = 1.85$ is chosen to resemble the redshift at which the cosmic SFH distribution peaks.

The bottom-half of Table C1 lists the γ values obtained by comparing the simulated parameters for both the fixed z_{crit} and fixed (α_l, α_u) cases with the observed FRBs from Parkes. Along with w_{obs} , we consider L_{obs} and E_{obs} as the independent parameters for the KS analysis in case of PL $n(z)$ as they are directly correlated with $S_{peak,obs}$ and \mathcal{F}_{obs} for a given z , which in turn depends on the specific $n(z)$ distribution. The value for equivalent KS is obtained from these parameters as $\gamma_{eq} = \sqrt{\gamma_{w_{obs}}^2 + \gamma_{L_{obs}}^2 + \gamma_{E_{obs}}^2}$. From the fixed (α_l, α_u) and varying z_{crit} case, we find that the agreement of each of the simulated w_{obs} , L_{obs} and E_{obs} distributions with the corresponding observed/inferred quantities from Parkes is considerably better for a smaller value of peak redshift for the FRB PL spatial density with $\gamma_i(z_{crit} = 1.0) > \gamma_i(z_{crit} = 2.0) > \gamma_i(z_{crit} = 3.0)$ for $i = w_{obs}, L_{obs}, E_{obs}$ and most of the cases considered.

Moreover, for the fixed z_{crit} and varying (α_l, α_u) case, we find that the observed w_{obs} and inferred E_{obs} from Parkes

Table 3. The follow-up observation information for repeating FRB 121102 and non-repeating FRBs from Table 1. The redshift z and burst energy E_{obs} are inferred by assuming a fixed host galaxy DM contribution $DM_{host} = 100 \text{ pc cm}^{-3}$. None of the 22 listed FRBs were observed to repeat inspite of dedicated follow-up efforts ranging from few hours to ~ 1000 hours.

FRB	Telescope	$S_{peak,obs}$ (Jy)	\mathcal{F}_{obs} (Jy ms)	z	E_{obs} (10^{42} erg)	t_{obs} (hr)	Reference
010621	Parkes	0.53	4.24	0.20	0.03	15.5	Keane et al. (2012)
090625	Parkes	1.14	2.19	1.06	0.53	33.65	Champion et al. (2016)
110220	Parkes	1.11	7.31	1.12	1.94	1.75	Thornton et al. (2013)
110626	Parkes	0.63	0.89	0.81	0.12	11.25	Thornton et al. (2013)
110703	Parkes	0.45	1.75	1.33	0.65	10.1	Thornton et al. (2013)
120127	Parkes	0.62	0.75	0.61	0.06	5.5	Thornton et al. (2013)
121002	Parkes	0.43	2.34	2.00	1.86	10.25	Champion et al. (2016)
121102	Arecibo, GBT, Effelsberg			0.19		235.7	†
130626	Parkes	0.74	1.47	1.09	0.37	9.5	Champion et al. (2016)
130729	Parkes	0.22	3.43	1.01	0.75	10	Champion et al. (2016)
131104	Parkes	1.16	2.75	0.85	0.43	78	Ravi et al. (2015)
140514	Parkes	0.47	1.32	0.62	0.11	19.2	Petroff et al. (2015b)
150215	Parkes	0.70	2.02	0.82	0.28	17.5	Petroff et al. (2017)
151206	Parkes	0.30	0.90	2.28	0.90	22.3	Bhandari et al. (2018)
151230	Parkes	0.42	1.90	1.13	0.52	54.9	Bhandari et al. (2018)
160317	UTMOST	3.0	63.00	1.03	14.32	105	Caleb et al. (2017)
160608	UTMOST	4.3	38.70	0.51	2.05	35	Caleb et al. (2017)
170107	ASKAP	22.3	57.98	0.68	5.64	669.6	Shannon et al. (2018)
170416	ASKAP	19.4	97.00	0.56	6.30	388.8	Shannon et al. (2018)
170428	ASKAP	7.7	34.00	1.17	9.92	758.4	Shannon et al. (2018)
171116	ASKAP	19.6	63.00	0.69	6.32	1096.8	Shannon et al. (2018)
180110	ASKAP	128.1	420.00	0.82	59.18	904.8	Shannon et al. (2018)
180131	ASKAP	22.2	100.00	0.74	11.46	758.4	Shannon et al. (2018)

† The follow-up data for the repeating FRB 121102 is obtained from Spitler et al. (2016), Scholz et al. (2016), Scholz et al. (2017), Law et al. (2017), Hardy et al. (2017), Michilli et al. (2018), Gajjar et al. (2018) and Spitler et al. (2018).

can be better explained with a FRB spatial density that gradually decreases with the source distance as $\gamma[(\alpha_l, \alpha_u) = (0, -3)] > \gamma[(\alpha_l, \alpha_u) = (0, 0)] > \gamma[(\alpha_l, \alpha_u) = (3, 0)]$ for both these burst parameters. In case of L_{obs} as well, a FRB $n(z)$ decreasing over distance is preferred by the current data with the likelihood order for PL indices being $(0, -3) > (3, 0) \sim (0, 0)$. Combining the results from the fixed (α_l, α_u) and fixed z_{crit} cases for PL $n(z)$ obtained here with those for SFH $n(z)$ in Section 4.1, we find that the FRB spatial density is likely to be a PL distribution with a peak around the redshift $z_{crit} \sim 1.0$. The reasonable agreement of the burst parameters with the observed FRB population at Parkes for SFH $n(z)$ also suggests PL indices $\alpha_l \approx 3.0$ and $\alpha_u \approx -3.0$ at asymptotically low and high redshifts, respectively. Here we have further constrained the decreasing FRB spatial densities at large distances to obtain an upper PL index $\alpha_u \sim -3.0$. Therefore, it is likely that the PL indices for the FRB spatial density are $\alpha_l \sim 0 - 3$ and $\alpha_u \approx -3$ with the distribution peaking at slightly smaller redshifts compared to the cosmic SFH.

5 FRB POPULATION AND REPEATABILITY

In Section 4, we constrained the FRB host galaxy DM, spectral index of the energy density, spatial distribution of the bursts and also the scattering due to turbulence in the intervening IGM and ISM using the observations for non-repeating/repeating bursts from Parkes/Arecibo. Now we use the follow-up data for FRBs in order to investigate whether FRB 121102 is representative of all FRBs repeating with a universal energy distribution function (EDF). Even though most FRBs have been extensively followed up with dedicated surveys ranging from few hours to ~ 1000 hrs, none of them except FRB 180814.J0422+73 were observed to be repeating. Table 3 lists the published follow-up observation data for the repeating FRB 121102 and 22 non-repeating FRBs from Table 1. There can be two possible reasons for the repeating bursts from other FRBs to not get detected inspite of a universal repetitive behaviour for FRBs: (a) the current observing times t_{obs} are smaller compared to the repeating timescale t_{rep} for the FRBs, or (b) the repeating bursts from the other FRBs are very dim and

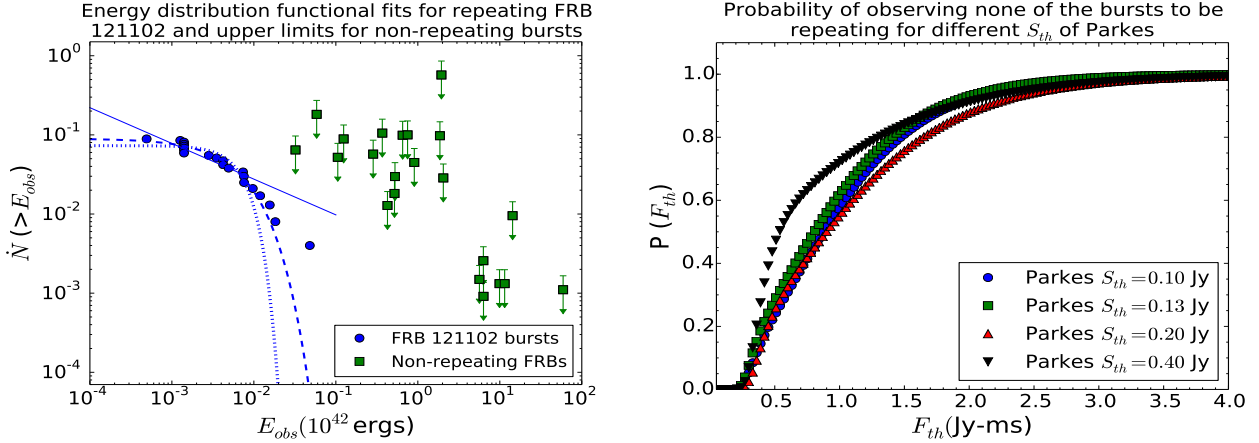


Figure 7. Follow-up observations for the repeating FRB 121102 and the non-repeating FRBs: Left panel: Power-law, exponential and gaussian fits for the CED of the repeating FRB 121102. The distribution for the repeater is normalized using its follow-up observing time $t_{obs} = 235.7$ hr. The upper limits for $\dot{N}(> E_{obs})$ of the 22 non-repeating FRBs are also shown and are normalized using their respective t_{obs} values from Table 3, Right panel: The probability of observing none of the 22 non-repeating FRBs to be repeating as a function of the fluence threshold \mathcal{F}_{th} (see equation 14). The probability is computed for different sensitivities of Parkes $S_{th} = 0.10, 0.13, 0.20, 0.40$ Jy.

cannot be detected with the typical sensitivities of the current telescopes.

The Parkes sensitivity threshold at $\nu_{obs} = 1.4$ GHz for $S/N = 9$ and an arbitrary w_{obs} is $S_{th} = 0.36$ Jy $(w_{obs}/1 \text{ ms})^{-1/2}$ (Caleb et al. 2016). For pulse widths in the range $w_{obs} \sim 1.00 - 8.00$ ms, S_{th} for Parkes varies within the range $\sim 0.1 - 0.4$ Jy. It should be noted that all the inferred energies in Table 1 are based on the lower limits for the fluence due to the uncertainty in the position of the source within a single beam and the assumption of on-axis detection for all bursts. Since Parkes is less sensitive as compared to Arecibo, we only include the repeating FRB 121102 sub-bursts for which $S_{peak,obs}$ exceeds the Parkes S_{th} for evaluating the repeater cumulative energy distribution (CED). Out of the 88 repeating bursts from FRB 121102 that we consider here, 65/55/46/21 bursts would have been above the Parkes $S_{th} \sim 0.10/0.13/0.20/0.40$ Jy at $\nu_{obs} = 1.4$ GHz.

The left-hand panel of Figure 7 shows the chi-squared PL, exponential and gaussian (with zero mean) fits for the CED of FRB 121102 along with the $\dot{N}(> E_{obs})$ upper limits for the non-repeating FRBs. While the repeating FRB CED is normalized with its total observing time $t_{obs} = 235.7$ hr, the $\dot{N}(> E_{obs,i})$ values for the individual non-repeating FRBs are normalized as $\dot{N}(> E_{obs,i}) = 1/t_{obs,i}$, where $t_{obs,i}$ is the observing time corresponding to the i -th burst. The best fit distribution for the CED of the repeating FRB is found to be: $\dot{N}_0 \exp(-E_{obs}/E_0)$ with $(\dot{N}_0, E_0) = (0.283 \text{ hr}^{-1}, 4.0 \times 10^{39} \text{ erg}) / (0.247 \text{ hr}^{-1}, 4.0 \times 10^{39} \text{ erg}) / (0.210 \text{ hr}^{-1}, 5.0 \times 10^{39} \text{ erg}) / (0.090 \text{ hr}^{-1}, 6.0 \times 10^{39} \text{ erg})$ for Parkes $S_{th} = 0.10/0.13/0.20/0.40$ Jy.

For each FRB, the threshold energy corresponding to a fluence completeness threshold \mathcal{F}_{th} is $E_{th}(z_i) = 4\pi D^2(z_i) \mathcal{F}_{th} (1+z_i) (\nu'_{max} - \nu'_{min})$. The average number of repeating events with energy $E \geq E_{th}(z_i)$ within time $t_{obs,i}$

for a burst at redshift z_i is

$$\begin{aligned} \bar{N}_{rep,i} &= \frac{t_{obs,i}}{(1+z_i)} \int_{E_{th}(z_i)}^{\infty} \frac{\dot{N}_0}{E_0} \exp\left(-\frac{E_{obs}}{E_0}\right) dE_{obs} \\ &= \frac{\dot{N}_0 t_{obs,i}}{(1+z_i)} \exp\left[-\frac{E_{th}(z_i)}{E_0}\right] \end{aligned} \quad (13)$$

If all other FRBs repeat at the same rate \dot{N}_0 as FRB 121102, the probability of observing none of the detected bursts to be repeating for a given value of \mathcal{F}_{th} is

$$\begin{aligned} P(\mathcal{F}_{th}) &= \prod_{i=1}^{22} \exp(-\bar{N}_{rep,i}) \\ &= \exp\left[-\sum_{i=1}^{22} \frac{\dot{N}_0 t_{obs,i}}{(1+z_i)} \exp\left(-\frac{E_{th}(z_i)}{E_0}\right)\right] \end{aligned} \quad (14)$$

In the right-hand panel of Figure 7, we show the variation of $P(\mathcal{F}_{th})$ within a range of \mathcal{F}_{th} for the 22 non-repeating FRBs with $t_{obs,i}$ listed in Table 3. We evaluate the $P(\mathcal{F}_{th})$ curves from equation (14) for the (\dot{N}_0, E_0) values corresponding to Parkes $S_{th} = 0.10/0.13/0.20/0.40$ Jy. The fluence completeness threshold for the Parkes FRBs was derived to be $\mathcal{F}_{th} \approx 2$ Jy ms by Keane & Petroff (2015).

We find that the probability of observing none of the 22 non-repeating FRBs that have been followed up so far to be repeating lies within the range $P(\mathcal{F}_{th}) \approx 0.8 - 1.0$ for $\mathcal{F}_{th} \approx 2$ Jy ms and Parkes $S_{th} \sim 0.1 - 0.4$ Jy. This is significantly larger than the probability $\sim 0.05 - 0.3$ obtained by Lu & Kumar (2016) for a smaller sample size and further supports repeating FRB as being representative of the entire FRB population. Although the follow-up observing times $t_{obs,i}$ have increased for the non-repeating FRBs now, the exponential EDF for the repeating FRB coupled to the difference in the mean E_{obs} for the non-repeating and repeating FRBs by almost three orders of magnitude implies that the other FRBs need to be followed up for significantly longer before concluding in favour of distinct FRB populations. It should however be noted that $t_{obs,i}$ for the FRBs are spread over different telescopes with a range of observ-

ing frequencies and sensitivities, and a more rigorous analysis regarding the repeatability of the FRBs would involve using a uniform sample which is possible once more bursts are followed up in the future.

6 SUMMARY AND CONCLUSIONS

In this paper, we described a formalism to study the intrinsic properties of the observed non-repeating and repeating FRBs and used MC simulations to constrain the properties of the FRB source, its host galaxy and the intervening turbulent medium from the current observational data. Although the physical origin of these events is still a matter of open debate with no concrete information about the progenitor model and/or radiation mechanism known at present, the population modelling of the FRB parameters helps in extracting useful information regarding the physical properties of these radio bursts from their observations. We have only considered FRBs with DM_{tot} exceeding 500 pc cm^{-3} that were published until January 2019 and derived their intrinsic properties self-consistently from the observations without assuming any initial distributions for the FRB parameters. The methods presented in this work can potentially be used in the near future in order to place even more tighter constraints on the burst properties and make observational predictions as the FRB population is expected to grow rapidly over the next few years with many radio transient surveys collecting more data.

We estimated the individual burst distances and intrinsic pulse widths by assuming a fixed host galaxy DM contribution and two scattering models for the temporal broadening due to multipath propagation of the pulse through ionized plasma, respectively. While w_{ISM} is suppressed relative to w_{IGM} by the geometrical lever-arm factor $\sim 4f(1-f)$ for both scattering models, w_{IGM} for model 2 is based on a theoretical model for IGM turbulence as opposed to an observationally established empirical fit for model 1. After computing $S_{peak,int}$ from w_{int} and \mathcal{F}_{obs} , we obtained the bolometric luminosity and energy for the bursts for a flat FRB energy spectrum with coherent emission within frequency range $\nu'_{min} = 600 \text{ MHz}$ to $\nu'_{max} = 8 \text{ GHz}$. We obtained chi-squared fits for the cumulative distributions of w_{int} and L_{int} of the FRBs, and used them to constrain the physical properties of FRBs with our MC code.

It should be noted that a larger host galaxy DM contribution would result in a smaller inferred z from equation (1) leading to a correspondingly small DM contribution from the IGM. The IGM scatter broadening w_{IGM} will then decrease while $w_{ISM,host}$ from the host galaxy ISM increases. As $w_{ISM,host}$ is suppressed significantly relative to w_{IGM} by the geometrical lever-arm factor, there is a net increase in w_{int} with increase in DM_{host} . However, as w_{IGM} is almost two orders of magnitude smaller compared to w_{int} for both populations of FRBs (see Figure 4), the resultant increase/decrease in $w_{int}/S_{peak,int}$ is negligible and the reduction in the inferred L and E values from equation (7) can be ignored. Therefore, the w_{int} and L_{int} distributions derived for a typical MW-like host galaxy with $DM_{host} \approx 100 \text{ pc cm}^{-3}$ in Section 2 will not change appreciably. Similarly, the assumption of a flat FRB energy spectrum with $\alpha \approx 0$ within the frequency range $\nu'_{min} = 600 \text{ MHz}$ to

$\nu'_{max} = 8 \text{ GHz}$ does not affect the inferred luminosity values significantly relative to the $\alpha \approx -1.4$ case for the Kolmogorov turbulence spectrum.

The distances to the simulated bursts are initially determined from the FRB spatial density (NE/SFH/PL) and the IGM contributions to the DM and width of the pulse are computed using z . The host galaxy DM contribution is obtained by assuming it to be a MW-like galaxy and scaling DM_{NE2001} with the parameter $\beta \sim 0.1 - 10$. The telescope beam center flux density is then obtained for a PL FRB energy density $E_{\nu'} = k\nu'^{\alpha}$, observing frequency bandwidth $(\nu_1, \nu_2) = (\nu_0 - 0.5\nu_{bw}, \nu_0 + 0.5\nu_{bw})$ and FRB coherent emission frequency range $(\nu'_{min}, \nu'_{max}) = (600 \text{ MHz}, 8 \text{ GHz})$ from equation (10). We modelled the flux degradation due to finite telescope beam size using a Gaussian beam profile to obtain the $S_{peak,obs}$ from equation (11). The $S_{peak,obs}$ dependent S/N is computed for every simulated burst and the FRB is detected if its flux density exceeds the telescope sensitivity threshold.

We compare the properties of the simulated non-repeating/repeating FRBs with those observed at Parkes/Arecibo in order to constrain the host galaxy DM relative to MW β , PL energy density spectral index α , scattering in the intervening turbulent plasma and the spatial density $n(z)$ of the FRB sources. Lastly, we discuss whether repeating FRB 121102 is representative of the entire FRB population based on its repetition rate \dot{N}_0 and a universal EDF. In the following, we summarise the main results of this work:

- (i) The w_{int} for non-repeating (repeating) FRBs varies within a broad range $\sim 0.3 - 10 \text{ ms}$ ($\sim 0.1 - 8 \text{ ms}$) and the cumulative width distribution is an exponential function with a cutoff $w_{int,c} \sim 2.0 \text{ ms}$ ($\sim 1.6 \text{ ms}$), while L_{int} varies within $\sim 10^{43} - 10^{47} \text{ erg/s}$ ($\sim 10^{41} - 10^{43} \text{ erg/s}$) with an exponential cumulative distribution and cutoff $L_{int,c} \sim 2.0 \times 10^{45} \text{ erg/s}$ ($\sim 2.7 \times 10^{42} \text{ erg/s}$). The ISM contribution to the width broadening is significantly suppressed in comparison to w_{IGM} due to the geometry of the scattering medium along the line of sight to the FRB source with $w_{ISM,MW} \lesssim 10^{-3} \text{ ms}$ and $w_{ISM,host} \lesssim 10^{-6} \text{ ms}$ for non-repeating FRBs and $w_{ISM,host/MW} \lesssim 10^{-4} \text{ ms}$ for repeating FRBs. As a result, the pulse width broadening due to scattering $w_{sc} \approx w_{IGM}$ for both classes of bursts. The scatter broadening of the pulse is found to be the smallest contribution to the w_{obs} with $w_{sc} \lesssim 1 \text{ ms}$ ($w_{sc} \lesssim 2 \times 10^{-2} \text{ ms}$) for the non-repeating (repeating) bursts. We find that w_{int} is largely scattering model independent for both classes of FRBs, and the average relative temporal broadening $\Delta w_{int}/w_{int} \sim 150\%$ and $\sim 20\%$ for non-repeating and repeating bursts, respectively. While w_{DM} is the dominant contribution to the temporal broadening for non-repeating FRBs with $w_{obs} \sim w_{int} \sim w_{DM} \gg w_{sc}$, the dispersive smearing in case of repeating bursts is significantly smaller with $w_{obs} \approx w_{int} \gg w_{DM} \gg w_{sc}$. Due to the small $z \approx 0.19273$ for FRB 121102, w_{sc} and w_{DM} contributions are found to be almost negligible and a considerable fraction of w_{obs} is expected to come from w_{int} .
- (ii) We find that the SFH spatial density is preferred over the NE spatial density based on the current Parkes observations reported at $\nu_{obs} = 1.4 \text{ GHz}$. However, the current

FRB observations from Parkes do not provide a sufficiently large data sample in order to distinguish substantially between the two IGM scattering broadening models considered here. The DM contribution from the host galaxy of the FRB source is expected to be either smaller or comparable to the Galactic contribution with $\beta \sim 0.1 - 1$. The Parkes observations for the non-repeating FRBs favour a large negative value of the FRB energy density spectral index α within the range -3.0 to -1.5.

We also compared the simulated FRB parameters with the Parkes data to constrain the peak redshift and low/high- z PL indices of the FRB spatial density. The spatial density of FRBs is likely to be a PL distribution peaking at smaller redshifts $z_{crit} \sim 0.5 - 1.0$ compared to the cosmic SFH. The FRB density is expected to increase upto $z \approx z_{crit}$ with a PL index $\alpha_l \sim 0 - 3$ and drop considerably at larger distances with $\alpha_u \approx -3$.

- (iii) We used the published FRB follow-up observing data in order to investigate whether FRB 121102 is representative of the entire population. The CED for the repeating FRB was computed by only including the FRB 121102 bursts for which $S_{peak,obs}$ exceeds the Parkes S_{th} . We obtained an exponential CED $\dot{N}_0 \exp(-E_{obs}/E_0)$, with repetition rate $\dot{N}_0 \sim 0.090 - 0.283 \text{ hr}^{-1}$ and cutoff energy $E_0 \sim (4 - 6) \times 10^{39} \text{ erg}$ for Parkes $S_{th} \sim 0.1 - 0.4 \text{ Jy}$. We find that if all FRBs repeat at the same rate $\dot{N}_0 \sim 0.090 - 0.283 \text{ hr}^{-1}$ and with a universal EDF, the probability of observing none of them to be repeating is $\sim 0.8 - 1.0$ for $\mathcal{F}_{th} \approx 2 \text{ Jy} - \text{ms}$ and Parkes $S_{th} \sim 0.1 - 0.4 \text{ Jy}$. As the universal EDF is an exponential distribution with a cutoff energy that is much smaller compared to the typical non-repeating FRB energies, significantly longer FRB follow-up observations are needed to distinguish between the FRB populations.

ACKNOWLEDGMENTS

We thank Siddhartha Bhattacharyya, Akshaya Rane, Wenbin Lu, Somnath Bharadwaj and Apurba Bera for useful discussions.

REFERENCES

- Bannister K. W., et al. 2017, *ApJ*, 841, L12
 Bera A., Bhattacharyya S., Bharadwaj S., Bhat N. D. R., Chennagur J. N., 2016, *MNRAS*, 457, 2530
 Bhandari S., et al. 2018, *MNRAS*, 475, 1427
 Bhat N. D. R., Cordes J. M., Camilo F., Nice D. J., Lorimer D. R., 2004, *ApJ*, 605, 759
 Caleb M., Flynn C., Bailes M., Barr E. D., Hunstead R. W., Keane E. F., Ravi V., van Straten W., 2016, *MNRAS*, 458, 708
 Caleb M., et al. 2017, *MNRAS*, 468, 3746
 Champion D. J., Petroff E., Kramer M., et al. 2016, *MNRAS*, 460, L30
 Chatterjee S., Law C. J., Wharton R. S., et al. 2017, *Nature*, 541, 58
 CHIME/FRB Collaboration, et al. 2019, *arXiv:1901.04525*
 Connor L., Sievers J., Pen U.-L., 2016, *MNRAS*, 458, L19
 Cordes J. M., Lazio T. J. W., 2002, preprint ([astro-ph/0207156](#))
 Cordes J. M., Wasserman I., 2016, *MNRAS*, 457, 232
 Deng W., Zhang B., 2014, *ApJ*, 783, L35
 Falcke H., Rezzolla L., 2014, *A&A*, 562, A137
 Gajjar V., Siemion A. P. V., Price D. C., et al. 2018, *ApJ*, 863, 2
 Gao H., Li Z., Zhang B., 2014, *ApJ*, 788, 189
 Hardy L. K., et al. 2017, *MNRAS*, 472, 2800
 Hassall T. E., Keane E. F., Fender R. P., 2013, *MNRAS*, 436, 371
 Inoue S., 2004, *MNRAS*, 348, 999
 Ioka K., 2003, *ApJL*, 598, L79
 Kashiyama K., Ioka K., Meszaros P., 2013, *ApJ*, 776, L39
 Kashiyama K., Murase K., 2017, *ApJL*, 839, L3
 Katz J. I., 2014, *Phys. Rev. D*, 89, 103009
 Katz J. I., 2016, *ApJ*, 826, 226
 Keane E. F., et al. 2012, *MNRAS*, 425, L71
 Keane E. F., Petroff E., 2015, *MNRAS*, 447, 2852
 Keane E. F., Johnston S., Bhandari S., et al. 2016, *Nature*, 530, 453
 Krishnakumar M. A., Mitra D., Naidu A., Joshi B. C., Manoharan P. K., 2015, *ApJ*, 804, 23
 Kulkarni S. R., Ofek E. O., Neill J. D., Zheng Z., Juric M., 2014, *ApJ*, 797, 70
 Kumar P., Lu W., Bhattacharya M., 2017, *MNRAS*, 468, 2726
 Law C. J., et al. 2017, *ApJ*, 850, 76
 Loeb A., Shvartzvald Y., Maoz D., 2014, *MNRAS*, 439, L46
 Lorimer D. R., Bailes M., McLaughlin M. A., Narkevic D. J., Crawford F., 2007, *Science*, 318, 777
 Lorimer D. R., Karastergiou A., McLaughlin M. A., Johnston S., 2013, *MNRAS*, 436, L5
 Lu W., Kumar P., 2016, *MNRAS*, 461, L122
 Lu W., Kumar P., 2018, *MNRAS*, 477, 2470
 Luan J., Goldreich P., 2014, *ApJ*, 785, L26
 Lyubarsky Y., 2014, *MNRAS*, 442, 9
 Lyutikov M., Burzawa L., Popov S. B., 2016, *MNRAS*, 462, 941
 Macquart J.-P., Koay J. Y., 2013, *ApJ*, 776, 125
 Madau P., Dickinson M., 2014, *ARA&A*, 52, 415
 Marcote B., Paragi Z., Hessels J. W. T., et al. 2017, *ApJL*, 834, L8
 Metzger B. D., Berger E., Margalit B., 2017, *ApJ*, 841, 14
 Michilli D., et al. 2018, *Nature*, 553, 182
 Mottez F., Zarka P., 2014, *A&A*, 569, A86
 Petroff E., Johnston S., Keane E. F., et al. 2015, *MNRAS*, 454, 457
 Petroff E., et al. 2015, *MNRAS*, 447, 246
 Petroff E., Barr E. D., Jameson A., et al. 2016, *PASA*, 33, e045
 Petroff E., et al. 2017, *MNRAS*, 469, 4465
 Piro A. L., 2012, *ApJ*, 755, 80
 Popov S. B., Postnov K. A., 2010, *Evolution of Cosmic Objects through their Physical Activity*. Publishing House of Nat. Acad. Sci. Rep. Armenia (NAS RA), Gitutyun, p. 129
 Rane A., Lorimer D. R., Bates S. D., McMann N., McLaughlin M. A., Rajwade K., 2016, *MNRAS*, 455, 2207
 Ravi V., Shannon R. M., Jameson A., 2015, *ApJL*, 799, L5
 Scholz P., et al. 2016, *ApJ*, 833, 177
 Scholz P., et al. 2017, *ApJ*, 846, 80
 Shannon R. M., et al. 2018, *Nature*, 562, 386
 Spitler L. G., Cordes J. M., Hessels J. W. T., et al. 2014, *ApJ*, 790, 101
 Spitler L. G., et al. 2016, *Nature*, 531, 202
 Spitler L. G., Herrmann W., Bower G. C., et al. 2018, *ApJ*, 863, 150
 Tendulkar S. P., Bassa C. G., Cordes J. M., et al. 2017, *ApJL*, 834, L7
 Thornton D., 2013, PhD thesis, The University of Manchester
 Thornton D., et al. 2013, *Science*, 341, 53
 Totani T., 2013, *PASJ*, 65, L12
 Vandenberg N. R., 1976, *ApJ*, 209, 578
 Williamson I. P., 1972, *MNRAS*, 157, 55
 Zhang B., 2014, *ApJ*, 780, L21
 Zhang B., 2017, *ApJL*, 836, L32

Zheng Z., Ofek E. O., Kulkarni S. R., Neill J. D., Juric M., 2014, *ApJ*, 797, 71

APPENDIX A: PULSE TEMPORAL BROADENING DUE TO IGM TURBULENCE

Here we derive the expression (equation 6) for the pulse temporal smearing due to IGM turbulence for the theoretical model proposed by [Macquart & Koay \(2013\)](#). The IGM temporal smearing w_{IGM} can be written in terms of the angular size of the image due to scatter broadening $\theta_{sc} = f D_{LS}/D_S k r_{diff}$ as

$$w_{IGM} = \frac{D_L D_S \theta_{sc}^2}{c D_{LS} (1 + z_L)} = \frac{f^2 \lambda_0^2}{c (1 + z_L)} \frac{D_{eff}}{4 \pi^2 r_{diff}^2} \quad (A1)$$

where $D_L/D_S/D_{LS}$ is the angular diameter distance from the observer to the scattering region/observer to the source/scattering region to the source, $z_L/z_S/z_{LS}$ is the corresponding redshift, $D_{eff} = D_L D_{LS}/D_S$ and $\lambda = 2\pi/k$ is the wavelength in the observer frame. We consider the case when the diffractive length scale r_{diff} is smaller compared to the inner scale of the scattering region l with the constant $f = 1.18$ to obtain $r_{diff} = (8.0 \times 10^9 \text{ m}) \lambda_0^{-1} \text{SM}_{eff,0}^{-1/2} l_0^{1/6}$, where $\lambda_0 = \lambda/(1 \text{ m})$, $\text{SM}_{eff,0} = \text{SM}_{eff}/(10^{12} \text{ m}^{-17/3})$ and $l_0 = l/(1 \text{ AU})$.

The z -corrected effective scattering measure is

$$\text{SM}_{eff}(z) = K_1 \int_0^z (1 + z')^3 d_H(z') dz' \quad (A2)$$

where $d_H(z') = (c/H_0)[\Omega_m(1 + z')^3 + \Omega_\Lambda]^{-1/2}$ and $K_1 \approx (9.42 \times 10^{-14} \text{ m}^{-20/3})$ is constant for the scattering region outer scale $L \sim 1 \text{ pc}$ and Kolmogorov turbulence spectrum. Substituting r_{diff} in terms of SM_{eff} into equation (A1) and further rewriting $\lambda_0 = c/\nu_0$ gives the temporal smearing (in sec)

$$w_{IGM}(z) = K_2 \frac{D_{eff}}{(1 + z_L)} \frac{\text{SM}_{eff}(z)}{\nu_0^4} \quad (A3)$$

where $K_2 \approx (1.56 \times 10^{-32} \text{ s})(f^2 c^3/4\pi^2)(l_0/1 \text{ AU})^{-1/3}$ is constant and ν_0 is the wave frequency in Hz in the observer frame.

Now we write D_{eff} and z_L in equation (A3) in terms of the source redshift z_S . We compute the maximum pulse temporal smearing assuming that the IGM scattering region is placed exactly midway along the source to the observed line of sight ([Vandenberg 1976](#); [Lorimer et al. 2013](#)), with $D_L = D_{LS}$ and $D_L = (1/2)D_S$ which further reduces to

$$\left(\frac{1 + z_{LS}}{1 + z_L} \right) \int_0^{z_L} d_H(z') dz' = \int_{z_L}^{z_S} d_H(z') dz' \quad (A4)$$

$$\frac{1}{(1 + z_L)} \int_0^{z_L} d_H(z') dz' = \frac{1}{2(1 + z_S)} \times \left(\int_0^{z_L} d_H(z') dz' + \int_{z_L}^{z_S} d_H(z') dz' \right) \quad (A5)$$

respectively. Substituting the second integral on the right-hand side of equation (A5) with equation (A4) and using $1 + z_{LS} = (1 + z_S)/(1 + z_L)$ gives the solution to the simultaneous equations (A4) and (A5) to be

$$1 + z_L = (1 + z)/(1 + z - \sqrt{z(1 + z)})$$

where we have replaced z_S with z . Lastly, using $D_{eff} = (1/4)D_S$ and $\text{SM}_{eff}(z)$ from equation (A2) in equation (A3) gives

$$w_{IGM}(z) = \frac{k_{IGM}}{\nu_{0,GHz}^4 Z_L} \int_0^z \frac{dz'}{[\Omega_m(1 + z')^3 + \Omega_\Lambda]^{0.5}} \times \int_0^z \frac{(1 + z')^3}{[\Omega_m(1 + z')^3 + \Omega_\Lambda]^{0.5}} dz' \quad (A6)$$

where k_{IGM} is the redshift independent normalisation factor including K_1 and K_2 , $\nu_{0,GHz} = \nu_0/10^9$ and $Z_L = (1 + z)^2 [(1 + z) - \sqrt{z(1 + z)}]^{-1}$.

APPENDIX B: SIMULATION RESULTS FOR REPEATING FRB 121102

Here we discuss the simulation results for the sub-bursts of the repeating FRB 121102 in order to better constrain the spectral properties of this source. In Figure A1, we show the results for the simulated $S_{peak,obs}$ and \mathcal{F}_{obs} distributions of the repeating bursts and further compare them with the Arecibo observations at $\nu_{obs} = 1.4 \text{ GHz}$. We fix the host galaxy DM contribution relative to MW β and the spatial density $n(z)$ model for all the simulations as the source redshift and the individual DM components (DM_{IGM} , DM_{MW} and DM_{host}) along the line of sight are both well known for FRB 121102. Also, we only consider model 1 for the IGM and ISM scattering in our simulations as the relative difference between the scattering models is found to be negligible for FRB 121102. We consider the value of the energy spectral index α to be varying within the range of -5.0 to 3.0, as supported by the current observations.

As $z = 0.19273$ is fixed for all the FRB 121102 bursts, the distribution for L_{obs}/E_{obs} is essentially the same as that for $S_{peak,obs}/\mathcal{F}_{obs}$ while the DM_{tot} is fixed. This reduces the number of independent parameters among the observed/inferred quantities to only two, and here we consider $S_{peak,obs}$ and \mathcal{F}_{obs} as the independent parameters for our analysis. Table A1 lists the γ values from the comparison of the simulated $S_{peak,obs}$ and \mathcal{F}_{obs} with the Arecibo $\nu_{obs} = 1.4 \text{ GHz}$ population. The equivalent KS value is obtained from the two observable parameters as $\gamma_{eq} = \sqrt{\gamma_{S_{peak,obs}}^2 + \gamma_{\mathcal{F}_{obs}}^2}$. We find that the observed $S_{peak,obs}$ for FRB 121102 bursts detected by Arecibo agree better with the simulated $S_{peak,obs}$ results for positive energy spectral indices, especially $\alpha \approx 2.0$. However, the observed \mathcal{F}_{obs} for the Arecibo bursts implies either a steep increasing or decreasing energy spectrum for this FRB. The γ_{eq} values obtained for FRB 121102 suggest a large negative $\alpha \sim -5.0$ to -4.0 or moderately positive $\alpha \sim 1.5$ to 2.0 for this repeating FRB. As a result, it is very unlikely that the repeating FRB 121102 has a flat energy spectrum across its entire emission range and its spectrum is expected to be better constrained in the future once more bursts are detected by Arecibo at $\nu_{obs} = 1.4 \text{ GHz}$ and their spectral information are available.

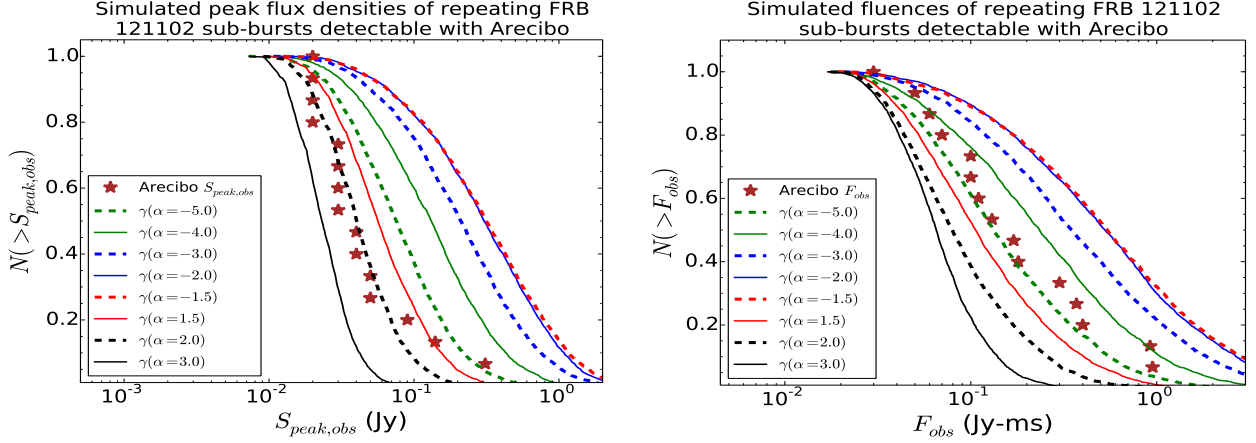


Figure A1. Comparison of repeating FRB sub-bursts detected by Arecibo at observing frequency $\nu_{obs} = 1.4$ GHz and simulated $S_{peak,obs}$ and \mathcal{F}_{obs} for FRB 121102 with different spectral indices. In both the panels, the MC simulation results are shown for α values ranging from -5.0 to 3.0. While β and $n(z)$ are fixed for the repeating FRB simulations, we only consider model 1 for the IGM and ISM scattering as the difference between the scattering models for the FRB 121102 sub-bursts is found to be negligible (see Section 2.3). *Left panel:* Simulation results for $S_{peak,obs}$ and different α , *Right panel:* Simulation results for \mathcal{F}_{obs} and different α .

Table A1. KS test values from the comparison of simulated $S_{peak,obs}$ and \mathcal{F}_{obs} with the observed repeating FRB 121102 sub-burst population detected at Arecibo with $\nu_{obs} = 1.4$ GHz. The γ values are obtained for a fixed β and $n(z)$ with $\gamma_{eq} = \sqrt{\gamma_{S_{peak,obs}}^2 + \gamma_{\mathcal{F}_{obs}}^2}$. All the values are listed for scattering model 1 as the difference between the intrinsic distributions is found to be insignificant between the two scattering models (see Table A3).

α	$\gamma_{S_{peak,obs}}$	$\gamma_{\mathcal{F}_{obs}}$	γ_{eq}
-5.0	0.001	0.970	0.686
-4.0	6.830×10^{-6}	0.258	0.182
-3.0	2.868×10^{-7}	0.023	0.016
-2.0	5.521×10^{-8}	0.003	0.002
-1.5	5.974×10^{-8}	0.002	0.001
1.5	0.028	0.489	0.346
2.0	0.448	0.043	0.318
3.0	0.004	4.829×10^{-4}	0.003

APPENDIX C: FRB INTRINSIC DISTRIBUTIONS AND KS ANALYSIS

Here we list the best fit distribution parameters for both non-repeating and repeating FRBs as well as the KS test values obtained from the comparison between simulated and observed FRB population at Parkes. Table A2 lists the functional fit parameters with the corresponding chi-squared values for the pulse width and luminosity of the non-repeating FRBs. The repeating FRB width and luminosity distribution fit parameters with the chi-squared values are listed in Table A3. The top-half of Table C1 lists the KS test values (γ) obtained from the comparison of the simulated parameters with those from the observed population at Parkes.

Table A2. Power-law, exponential and gaussian fit parameters for the width and luminosity distributions of non-repeating FRBs

Width	Distribution	Functional fit	Reduced χ^2
Observed	Power-law	$(35.431 \pm 2.538) w_{obs}^{-0.917 \pm 0.058}$	0.369
	Exponential	$(30.868 \pm 1.507) e^{-w_{obs}/(4.182 \pm 0.233)}$	0.135
	Gaussian	$(20.578 \pm 1.312) e^{-w_{obs}^2/2(4.102 \pm 0.271)^2}$	0.447
Intrinsic (1/2)	Power-law	$(13.220 \pm 0.496) w_{int1}^{-0.744 \pm 0.045} / (13.103 \pm 0.502) w_{int2}^{-0.736 \pm 0.045}$	0.342/0.356
	Exponential	$(25.369 \pm 1.044) e^{-w_{int1}/(2.086 \pm 0.122)} / (25.237 \pm 1.029) e^{-w_{int2}/(2.092 \pm 0.122)}$	0.141/0.140
	Gaussian	$(18.892 \pm 1.134) e^{-w_{int1}^2/2(1.838 \pm 0.132)^2} / (18.841 \pm 1.129) e^{-w_{int2}^2/2(1.839 \pm 0.132)^2}$	0.509/0.510
Luminosity	Distribution	Functional fit	Reduced χ^2
Observed	Power-law	$(12.916 \pm 0.867) L_{obs}^{-0.310 \pm 0.031}$	1.038
	Exponential	$(17.061 \pm 1.109) e^{-L_{obs}/(10.812 \pm 1.723)}$	0.666
	Gaussian	$(19.547 \pm 1.902) e^{-L_{obs}^2/2(2.517 \pm 0.375)^2}$	1.254
Intrinsic (1/2)	Power-law	$(17.468 \pm 0.999) L_{int1}^{-0.299 \pm 0.024} / (17.489 \pm 0.999) L_{int2}^{-0.298 \pm 0.024}$	0.928/0.927
	Exponential	$(18.203 \pm 1.339) e^{-L_{int1}/(21.588 \pm 4.385)} / (18.395 \pm 1.362) e^{-L_{int2}/(20.741 \pm 4.198)}$	0.657/0.654
	Gaussian	$(16.235 \pm 1.311) e^{-L_{int1}^2/2(13.368 \pm 2.098)^2} / (16.297 \pm 1.311) e^{-L_{int2}^2/2(13.206 \pm 2.047)^2}$	1.185/1.173

Table A3. Power-law, exponential and gaussian fit parameters for the width and luminosity distributions of repeating FRB

Width	Distribution	Functional fit	Reduced χ^2
Observed	Power-law	$(40.114 \pm 1.632) w_{obs}^{-0.657 \pm 0.033}$	5.255
	Exponential	$(93.887 \pm 0.757) e^{-w_{obs}/(2.135 \pm 0.023)}$	0.113
	Gaussian	$(71.173 \pm 1.438) e^{-w_{obs}^2/2(1.992 \pm 0.043)^2}$	0.973
Intrinsic (1/2)	Power-law	$(34.593 \pm 1.453) w_{int1/2}^{-0.656 \pm 0.032}$	5.026/5.026
	Exponential	$(94.407 \pm 0.842) e^{-w_{int1/2}/(1.628 \pm 0.019)}$	0.130/0.130
	Gaussian	$(71.762 \pm 1.523) e^{-w_{int1/2}^2/2(1.485 \pm 0.034)^2}$	1.061/1.061
Luminosity	Distribution	Functional fit	Reduced χ^2
Observed	Power-law	$(2.436 \pm 0.351) L_{obs}^{-0.593 \pm 0.028}$	4.228
	Exponential	$(89.749 \pm 1.013) e^{-L_{obs}/(0.020 \pm 0.001)}$	0.215
	Gaussian	$(70.157 \pm 1.817) e^{-L_{obs}^2/2(0.017 \pm 0.001)^2}$	1.579
Intrinsic (1/2)	Power-law	$(3.341 \pm 0.438) L_{int1/2}^{-0.548 \pm 0.026}$	4.471/4.471
	Exponential	$(86.169 \pm 0.989) e^{-L_{int1/2}/(0.027 \pm 0.001)}$	0.233/0.233
	Gaussian	$(68.484 \pm 1.940) e^{-L_{int1/2}^2/2(0.022 \pm 0.001)^2}$	1.906/1.906

Table C1. *KS test values γ from the comparison of simulated FRB parameters with the observed FRB population at Parkes.* The top-half of the table lists the values for w_{obs} , $S_{peak,obs}$ and DM_{tot} of the NE and SFH non-repeating FRB population. The γ values are obtained for different β and α combinations with $\gamma_{eq} = \sqrt{\gamma_{w_{obs}}^2 + \gamma_{S_{peak,obs}}^2 + \gamma_{DM_{tot}}^2}$. The values for scattering model 1/2 are listed for each entry. The bottom-half of the table lists the values for w_{obs} , L_{obs} and E_{obs} for PL population with varying z_{crit} or varying (α_l, α_u) . The γ values for the PL population are obtained for cases 1-5 given in Section 4.2 with $\gamma_{eq} = \sqrt{\gamma_{w_{obs}}^2 + \gamma_{L_{obs}}^2 + \gamma_{E_{obs}}^2}$.

$n(z)$	β	α	$\gamma_{w_{obs}}$	$\gamma_{S_{peak,obs}}$	$\gamma_{DM_{tot}}$	γ_{eq}
NE	0.1 (1.0) [10.0]	-3.0	0.352/0.376 (0.369/0.362) [0.161/0.204]	0.022/0.022 (0.031/0.022) [0.035/0.021]	0.020/0.019 (0.077/0.111) [0.009/0.008]	0.204/0.218 (0.218/0.219) [0.095/0.118]
		-1.5	0.138/0.142 (0.092/0.129) [0.048/0.060]	0.055/0.051 (0.074/0.054) [0.067/0.063]	0.047/0.051 (0.011/0.027) [4.939 $\times 10^{-6}$ /9.282 $\times 10^{-6}$]	0.090/0.092 (0.068/0.082) [0.048/0.050]
		1.5	0.036/0.043 (0.017/0.035) [0.017/0.016]	0.328/0.408 (0.271/0.481) [0.301/0.307]	3.103 $\times 10^{-4}$ /1.442 $\times 10^{-4}$ (4.659 $\times 10^{-5}$ /2.040 $\times 10^{-4}$) [2.253 $\times 10^{-7}$ /1.301 $\times 10^{-7}$]	0.191/0.237 (0.157/0.278) [0.174/0.177]
		3.0	0.007/0.004 (0.004/0.006) [0.002/0.003]	0.009/0.004 (0.003/0.008) [0.002/0.004]	2.136 $\times 10^{-5}$ /1.005 $\times 10^{-5}$ (5.505 $\times 10^{-6}$ /9.531 $\times 10^{-6}$) [1.454 $\times 10^{-8}$ /2.047 $\times 10^{-8}$]	0.007/0.003 (0.003/0.006) [0.002/0.003]
SFH	0.1 (1.0) [10.0]	-3.0	0.504/0.629 (0.512/0.627) [0.293/0.292]	0.004/0.002 (0.004/0.003) [0.003/0.004]	0.008/0.007 (0.022/0.030) [0.025/0.038]	0.291/0.363 (0.296/0.362) [0.170/0.170]
		-1.5	0.196/0.208 (0.193/0.217) [0.087/0.072]	0.028/0.024 (0.032/0.024) [0.036/0.024]	0.114/0.075 (0.050/0.054) [1.609 $\times 10^{-5}$ /1.073 $\times 10^{-5}$]	0.132/0.128 (0.117/0.130) [0.054/0.044]
		1.5	0.071/0.045 (0.046/0.074) [0.023/0.024]	0.440/0.362 (0.460/0.423) [0.406/0.395]	0.001/4.936 $\times 10^{-4}$ (4.936 $\times 10^{-4}$ /5.503 $\times 10^{-4}$) [5.595 $\times 10^{-7}$ /7.496 $\times 10^{-7}$]	0.257/0.211 (0.267/0.248) [0.235/0.228]
		3.0	0.009/0.021 (0.012/0.010) [0.010/0.008]	0.007/0.032 (0.012/0.009) [0.014/0.018]	8.772 $\times 10^{-5}$ /1.392 $\times 10^{-4}$ (8.462 $\times 10^{-5}$ /5.401 $\times 10^{-5}$) [1.850 $\times 10^{-7}$ /2.153 $\times 10^{-7}$]	0.007/0.022 (0.010/0.008) [0.010/0.011]
PL $n(z)$	(α_l, α_u)	z_{crit}	$\gamma_{w_{obs}}$	$\gamma_{L_{obs}}$	$\gamma_{E_{obs}}$	γ_{eq}
Case 1	(2.7,-2.9)	1.00 (2.00) [3.00]	0.897 (0.477) [0.410]	0.512 (0.649) [0.622]	0.545 (0.193) [0.186]	0.674 (0.478) [0.443]
Case 2			0.847 (0.395) [0.402]	0.556 (0.652) [0.694]	0.638 (0.184) [0.155]	0.691 (0.453) [0.472]
Case 3			0.923 (0.138) [0.015]	0.580 (0.089) [1.100 $\times 10^{-4}$]	0.694 (0.001) [2.543 $\times 10^{-7}$]	0.746 (0.095) [0.009]
Case 4			0.932 (0.138) [0.005]	0.679 (0.083) [1.153 $\times 10^{-4}$]	0.643 (0.001) [1.001 $\times 10^{-7}$]	0.762 (0.093) [0.003]
Case 5			0.672 (0.051) [0.005]	0.620 (0.094) [1.798 $\times 10^{-4}$]	0.822 (3.834 $\times 10^{-4}$) [3.138 $\times 10^{-7}$]	0.710 (0.062) [0.003]
Case 1	(0,-3){3,0} [0,0]	1.85	0.788 {0.479} [0.856]	0.267 {0.640} [0.287]	0.336 {0.210} [0.369]	0.518 {0.477} [0.563]
Case 2			0.692 {0.413} [0.728]	0.263 {0.607} [0.289]	0.433 {0.188} [0.421]	0.495 {0.438} [0.513]
Case 3			0.786 {0.177} [0.253]	0.864 {0.127} [0.121]	0.489 {0.003} [0.012]	0.731 {0.126} [0.162]
Case 4			0.860 {0.165} [0.253]	0.964 {0.115} [0.111]	0.640 {0.002} [0.016]	0.832 {0.116} [0.160]
Case 5			0.491 {0.086} [0.120]	0.942 {0.218} [0.128]	0.389 {0.002} [0.013]	0.653 {0.135} [0.102]